Eur. J. Mineral.
2004, **16**, 451–468

Computer simulation of octahedral cation distribution and interpretation of the Mössbauer Fe^{2+} components in dioctahedral trans-vacant micas

LIDIA G. DAINYAK[1]*, VICTOR A. DRITS[1] and HOLGER LINDGREEN[2]

[1]Geological Institute of the Russian Academy of Science, Pyjzhevsky Street 7, 109017 Moscow, Russia
*Corresponding author, e-mail: dainyak@ginras.ru
[2]Geological Survey of Denmark and Greenland, Øster Voldgade 10, 1350 Copenhagen K, Denmark

Abstract: Cation distributions (CDs) in the representative collection of trans-vacant dioctahedral celadonites, glauconites and ferriillites were investigated using Mössbauer and IR spectroscopies and the original approach. The approach is based on individual quadrupole splittings Δ_i^{pred} for Fe^{3+} in possible local cation arrangements around Fe^{3+}, and on a computer simulation of two-dimentional CDs using the IR data in the OH stretching vibration region.

The resulting CDs were next used to make correlations between Δ_j of Fe^{2+} derived from computer fits to the corresponding spectra and cation composition of local cation arrangements around Fe^{2+} with their occurrence probabilities. Basing on this correlations, a total of eight individual Δ_i^{tent} for Fe^{2+} referred as "tentative" have been derived.

The order of local cation arrangements in terms of increasing quadrupole splitting was found to be the same both for Fe^{3+} and Fe^{2+} and implies a direct dependence of the Fe^{2+} quadrupole splitting on the structural distortion at Fe^{2+} site.

The set of Δ_i^{tent} for Fe^{2+} combined with Δ_i^{pred} for Fe^{3+} and with the new CD simulation program provide an additional means for controlling the CD reconstruction.

Key-words: Mössbauer spectroscopy, dioctahedral micaceous minerals, computer simulation, cation distribution.

1. Introduction

Dioctahedral potassium micas and their fine dispersed micaceous minerals (phengites, illites, glauconites, celadonites, leucophillites) are important rock-forming minerals and their structural and crystal chemical features are used as indicators of physico-chemical conditions of formation and transformation of these minerals in sediments and rocks.

The basic structural unit of the micas is a 2:1 layer in which a sheet consisting of edge sharing octahedra is sandwiched between two sheets of corner sharing Si, Al tetrahedra. A 2:1 layer unit cell contains one trans-, or T-octahedron, and two, CI and CII, cis-octahedra, which differ from each other by arrangement of hydroxyl groups. Adjacent CI and CII octahedra share an edge formed by two OH groups whereas in the T-octahedra hydroxyls are located opposite each other. Positions of cations located in T, CI and CII octahedra are denoted as M1, M2 and M2', respectively. In dioctahedral micas and micaceous minerals, T, CI, or CII octahedron is vacant (Bailey, 1984; Drits *et al.*, 1993 a). In trans-vacant (tv) micas M2 and M2' sites are equivalent or non-equivalent depending on the unit cell symmetry. In the first case the unit cell has a mirror plane, two-fold axis and *C*2/*m* group of symmetry and in the second only a two-fold axis and *C*2 group, respectively.

A characteristic feature of dioctahedral micas is a wide spectrum of isomorphous substitutions of various cations in the octahedral and tetrahedral sheets. Spectroscopic methods and Mössbauer spectroscopy in particular are very important for determination of isomorphous cation distribution since they probe local cation environments and can detect short-range order in cation arrangements. For a long time, each individual doublet in Mössbauer spectra was assumed to correspond to a single crystallographic site. Therefore, Mössbauer spectra of Fe^{3+}-bearing dioctahedral micas were decomposed into two main doublets. One was assigned to Fe^{3+} in trans-sites and the second one to Fe^{3+} in cis-sites (see, for example, review by Heller-Kallai & Rosenson, 1981). Application of X-ray and electron diffraction methods has shown that Fe-rich dioctahedral layer silicates such as Fe-illites, glauconites, celadonites and nontronites consist only of tv layers (Drits *et al.*, 1984; Tsipursky *et al.*, 1985; Tsipursky & Drits, 1984; Sakharov *et al.*, 1990, Besson *et al.*, 1983; Drits & McCarty; Manceau *et al.*, 1998, 2001; Cuadros, 2002). Therefore, the conventional interpretation of the Mössbauer spectra had to be revised, and more than two decades ago, we began developing an approach to the interpretation of Fe^{3+} components in the Mössbauer spectra of dioctahedral micaceous minerals based on the cation distribution (CD) in the unit cell determined by X-ray and electron diffraction (Bookin *et al.*, 1978; Dainyak *et al.*, 1981; Besson *et al.*, 1983; Dainyak *et al.*, 1984 a, b, and c;

DOI: 10.1127/0935-1221/2004/0016-0451
0935-1221/04/0016-0451 $ 8.10

Dainyak & Drits, 1987; Dainyak *et al.*, 1992; Drits *et al.*, 1997). The assumption of this approach is that the observed difference in quadrupole splittings of Fe^{3+} cations is caused by the distortion of Fe^{3+} octahedra due to local cation environments around these cations. In this case the number of doublets in the Mössbauer spectra does not correlate with the number of crystallographic sites but depends on the number of different cation arrangements around a crystallographic site. The important role of these local effects is acknowledged by many authors (Goodman, 1976a, 1987; Mineeva, 1978; Johnston & Cardile, 1985; Redhammer, 1998; Redhammer *et al.*, 2000, 2002).

Computer simulation of the two-dimensional octahedral CD (Dainyak *et al.*, 1992) using IR data on the distribution of cations around the OH groups (Slonimskaya *et al.*, 1986; Besson & Drits, 1997 a and b) has proved to be very useful for understanding the Mössbauer spectra.

Until now, this work has focused on the distribution of Fe^{3+}, which is generally the main form of iron, in dioctahedral aluminosilicate minerals. Its electric field gradient (EFG), which determines the quadrupole splitting in Mössbauer spectra, is determined largely by the distribution of charges in the mineral lattice, q_{lat} (see, for example, Greenwood & Gibb, 1971; Bancroft, 1974; Coye, 1980). The interpretation of quadrupole splittings for the minor Fe^{2+} doublets is more difficult because of the main valence contribution, q_{val}, to the EFG at Fe^{2+} cations, but this should also be based on diffraction data on cation distribution in the unit cell.

The possibility that there were variations in the atomic orbital composition of Fe^{2+} ions in aluminosilicate minerals as a result of differences in the distributions of neighbouring cations was first considered by Goodman (1976 a), who proposed that q_{val} at Fe^{2+} sites contains contributions from valence electrons, which vary according to the local structure around the iron. However, in EFG calculations, which were based on trioctahedral minerals, Goodman assumed a random distribution of octahedral cations and similar lattice contributions, q_{lat}, to the quadrupole splittings at both Fe^{3+} and Fe^{2+} sites. Both of these assumptions are questionable (B. Goodman, personal communication).

Recently, Shabani *et al.* (1998) studying Mössbauer spectra of dioctahedral $2M_1$ micas conventionally assigned two Fe^{2+} doublets observed in the spectra to trans- and cis-sites but noted simultaneously a domination of local effects.

In the present study, we have modified the computer program for the CD simulation model, which was originally applied to Fe^{3+} ions (Dainyak *et al.*, 1992), to enable the study of Fe^{2+} ions in dioctahedral minerals, where they are generally minor components. These calculations use data from IR and Mössbauer spectroscopic studies of a collection of well-characterized dioctahedral trans-vacant micaceous minerals. They proceed in two stages. Firstly, two-dimensional CDs are derived for the Fe^{3+} components. Then by using the elemental compositions of the minerals, correlations are made between the various arrangements of the cations nearest to Fe^{2+} and the Fe^{2+} quadrupole splittings derived from computer fits to the corresponding Mössbauer spectra. Thus, for the first time, the Fe^{2+} quadrupole doublets are interpreted in terms of the local structure in dioctahedral micas.

Table 1. Parameters of the equation predicting the individual Δ_i^{pred} values, by Drits *et al.* (1997)*.

Arrangement	$3\text{-}Z^{av}$	d^{av}	Δ_i^{pred}, mm/s
$3Fe^{2+}$	1.	2.12	0.
$2Fe^{2+}Mg$	1.	2.103	0.13
$3Fe^{3+}$	0.	1.98	0.17
$2MgFe^{2+}$	1.	2.087	0.26
$2Fe^{2+}Fe^{3+}$	0.	1.96	0.33
$2Fe^{3+}Al$	0.667	2.073	0.34
3Mg	1.	2.07	0.39
$2Fe^{2+}Al$	0.667	2.057	0.48
$MgFe^{2+}Fe^{3+}$	0.667	2.057	0.49
$2AlFe^{3+}$	0.	1.947	0.51
$2MgFe^{3+}$	0.667	2.04	0.61
$AlMgFe^{2+}$	0.667	2.04	0.63
$2Fe^{3+}Fe^{2+}$	0.333	2.027	0.65
2MgAl	0.	1.93	0.74
$AlFe^{2+}Fe^{3+}$	0.667	2.023	0.78
$2Fe^{3+}Mg$	0.333	2.01	0.79
3Al	0.333	2.01	0.86
$AlMgFe^{3+}$	0.333	1.993	1.02
$2AlFe^{2+}$	0.333	1.993	1.06
2AlMg	0.333	1.977	1.40

* Z^{av} and d^{av} are charge and the bond length averaged over three charges and three mean lengths, respectively, in the three octahedra nearest to Fe^{3+}. The mean bond lengths $d(Fe^{3+}) = 1.98$ Å, $d(Fe^{2+}) = 2.12$ Å, $d(Mg) = 2.07$ Å , and $d(Al) = 1.93$ Å (Drits, 1975; Smoliar-Zviagina, 1993).

2. Strategy adopted for interpreting the Mössbauer spectra

Because of the sensitivity of Mössbauer spectroscopy to the local order-disorder in the distribution of octahedral isomorphous cations around Fe, the first step in our approach is to examine the various arrangements of the three nearest octahedral cations around the Fe in the octahedral sheet. For four types of octahedral cations (Al, Fe^{3+}, Fe^{2+}, Mg), there are 20 local cation arrangements ($3Fe^{3+}$, 3Al, $2AlFe^{3+}$ *etc.*) (Table 1).

The individual Fe^{3+} doublets, which correspond to these various structural arrangements, are not resolved in the Mössbauer spectra, because of the small differences in their spectral parameters compared to the linewidth. Thus spectra consist of groups of closely overlapping peaks, from which statistically acceptable fits can usually be obtained with between two and four broadened Lorentzian doublets. By working with sample sizes which approximate to the thin absorber condition, and assuming the same recoil-free fraction values for Fe^{3+} in the different local arrangements, each of these "experimental" j doublets may be considered to be a superposition of individual doublets with a small range of quadrupole splittings, Δ_i. Each Δ_i corresponds to a definite local cationic arrangement with occurrence probabilities, w_i. An empirical equation for the assignment of the Δ_i values to the local arrangements has been reported by Drits *et al.* (1997), and this is used in the present work. Using these predicted Δ_i values, the problem of determining the "fine structure" of the j doublets fitted to the spectrum can be

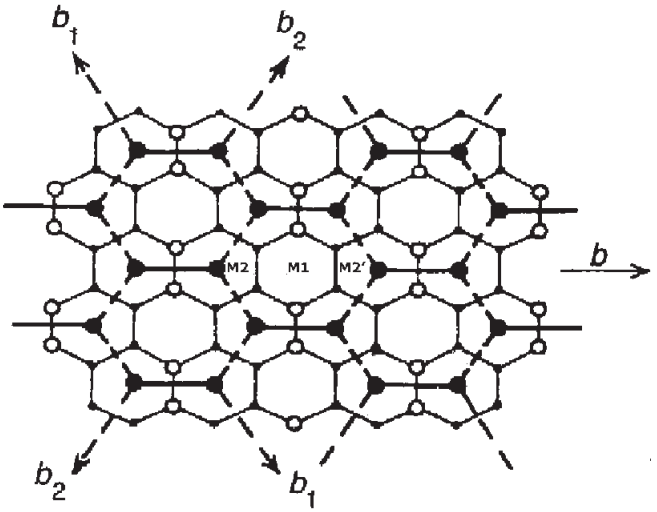

Fig. 1. Two-dimensional distribution of cations in a trans-vacant octahedral sheet. Solid and dashed lines connecting cations correspond to the ***b*** axis and $\boldsymbol{b_1}$ and $\boldsymbol{b_2}$ direction, respectively. Open and black large circles correspond, respectively, to OH groups and octahedral cations occupying *cis*-sites.

solved by simulation of two-dimensional CD. The aim of this work, therefore, is to generate CD reconstructions, which satisfy both the relative areas S_j and Δ_j values of the Mössbauer spectra

Since the EFG on Fe^{3+} is determined to a good approximation by lattice contributions, q_{lat}, it increases with increasing local distortion (Bancroft, 1974; Coey, 1980). This is assumed in the empirical equation of Drits *et al.* (1997), where the Δ_i^{pred} values are calculated taking account of the charge, Z^{av}, and the bond length, d^{av}, averaged over three charges and three mean bond lengths, respectively, in three octahedra nearest to Fe^{3+}. Table 1 shows the local cationic arrangements in order of increasing individual Δ_i^{pred} values, along with the corresponding $(3–Z^{av})$ and d^{av} values. For arrangements which are homogeneous by charge $(3 - Z^{av}) = 0$, Δ_i^{pred} increases with decreasing d^{av}. The Δ_i^{pred} values for the other arrangements result from a combination of charge and size heterogeneity. The mean M-O,OH bond lengths typical for Fe^{3+}-, Fe^{2+}-, Mg- and Al-octahedra in dioctahedral 2:1 layer silicates (Drits, 1975; Smoliar-Zviagina, 1993) are given in Table 1.

The equation predicts quadrupole splittings equal to 0.74 and 0.17 mm/s for the 3Al and $3Fe^{3+}$ arrangements, respectively. These values are observed in Mössbauer spectra of Fe^{2+}-free muscovite containing a low amount of Fe^{3+} (Goodman, 1976 b) and ferripyrophyllite (Coey *et al.*, 1984). In addition, investigation by chemical analysis, IR and Mössbauer spectroscopies of a unique glauconite sample having an anomalous high content of Fe^{2+} showed that $\Delta \approx 0$ mm/s corresponds to the $3Fe^{2+}$ local cation arrangement (Zaitseva, in preparation).

Reliability of the Δ_i^{pred} values predicted by the equation is also justified by the fact that CD distributions simulated according to these values for celadonites, glauconites and Fe^{3+}- illites satisfied experimental data obtained by EXAFS and IR spectroscopies and chemical analysis (Drits *et al.*, 1997). Analysis of CD reconstructions for these minerals revealed specific features, such as the clustered structure of glauconites and the non-equivalent cation occupancy of M2 and M2' sites in respect of R^{2+} and R^{3+} content. These results were corroborated by the observation of ferromagnetic ordering at 1.3 K in glauconite (Townsend *et al.*, 1987). Consequently, this model is considered to be a reliable basis for the current work.

3. Simulation of two-dimensional octahedral cation distributions to satisfy the parameters from computer fits to Mössbauer spectra

The computer program described by Dainyak *et al.* (1992) for simulating two-dimensional octahedral cation distributions made use of integrated IR optical densities for bands W_{ik}, where i and k (Al, Fe^{3+}, Fe^{2+} and Mg) are the cations bound to the OH groups (Slonimskaya *et al.*, 1986; Besson & Drits, 1997 a and b). Since the W_{ik} values are proportional to the sum of the occurrence probabilities, w_{ik} and w_{ki}, the individual occupancy of M2 and M2' sites (Fig. 1) for any cation pair can either be equal or show a preference of one cation for one of the sites. For example, if the W_{AlMg} value for the cationic pair AlMg is 0.3 and Mg prefers the M2' site, then we have $w_{AlMg} = 0.3$ and $w_{MgAl} = 0$. As the direction of adjacent occupied octahedra in tv 2:1 layers coincides with the ***b***-direction (Fig. 1), the corresponding cation pairs can be referred to as ***b***-oriented.

The simulation program used a heuristic algorithm, consisting of two stages. The first stage is the random filling of the honeycomb pattern of the dioctahedral sheet with ***b***-oriented cation pairs with pre-set occurrence probabilities, w_{ik} and w_{ki}. The second "improvement" stage refines these cation distributions.

In the first version of the program, this latter stage used the penalty function

$$f(\alpha) = \alpha N_{FA} + (1 - \alpha) N_{22},$$

where α was pre-set and N_{FA} and N_{22} were the numbers of $Fe^{3+}Al$ and $R^{2+}R^{2+}$ pairs in directions $\boldsymbol{b_1}$ and $\boldsymbol{b_2}$ (Fig. 1), respectively. This function, referred to as "diagonal limitation", regulated the occurrence of the $\boldsymbol{b_1}$- and $\boldsymbol{b_2}$-oriented $Fe^{3+}Al$ and $R^{2+}R^{2+}$ pairs for each of these directions. Thus, different restrictions on N_{FA} and N_{22} led to various CD models characterized by the individual occurrence probabilities, w_i, for the local arrangements of three cations nearest to the Fe^{3+}. For each model, the w_i values corresponding to the cation arrangements with similar Δ_i^{pred} values were arbitrarily grouped into j groups in accordance with the number of fitted doublets in the spectrum. Within each of these groups, the sum $W_j = \Sigma_i w_i$ and statistically weighted $\Delta^{calc} = \Sigma_i w_i^{norm} \cdot \Delta_i^{pred}$ were found. The W_j and Δ_j^{calc} values were then compared with Mössbauer fitted parameters S_j and Δ_j, where S and Δ are the area and quadrupole splitting, respectively. If agreement was good then the CD model was accepted and the Mössbauer spectrum considered to be interpreted. If not, then the simulation was repeated with new values until agreement was obtained. These calculations were, therefore, both time-consuming and labour-intensive.

Table 2. Cation composition of the studied samples calculated for $O_{10}(OH)_2$.

Sample	1 69g	2 68/69*	3 e8/2	4 40/7	5 Ch	6 B.Pat*	7 136	8 60
Cation								
Si	3.94	3.78	3.65	3.70	3.42	3.46	4.	3.63
Al^t	0.06	0.22	0.35	0.30	0.58	0.54		0.37
Al^{oct}	0.05	0.55	0.68	0.87	0.92	1.11	1.05	1.41
Fe^{3+}	1.15	0.89	0.79	0.64	0.74	0.41	0.17	0.10
Fe^{2+}	0.36	0.18	0.10	0.20	0.07	0.13	0.21	0.07
Mg	0.41	0.39	0.43	0.29	0.27	0.35	0.59	0.42
Σ_{0ct}	1.97	2.01	2.	2.	2.	2.	2.02	2.
K	0.83	0.80	0.78	0.62	0.79	0.74	0.72	0.77
Na	0.01		0.01	0.03	0.02	0.01	0.01	0.07
Ca	0.03		0.03	0.02	0.05	0.06		0.01
Mg				0.03		0.07		
Σ_{int}	0.87	0.80	0.82	0.79	0.86	0.88	0.73	0.85

Key: 1 – celadonite (Pavlishin *et al.*, 1978; Drits *et al.*, 1993 b); 2 – glauconite (Shutov *et al.*, 1975; Drits and Kossovskaya, 1992); 3 – glauconite (Nicolaeva, 1977; Drits *et al.*, 1993); 4 – glauconite (Ivanovskaya *et al.*, 1989); 5 – Fe-illite from illite stratum, Syria, given by V.I. Muraviev (GIN RAN, Moscow); 6 – Fe-illite (Nikolaeva, 1977; Drits *et al.*, 1993); 7 – leucophyllite (Raskazov, 1984); 8 – illite (Ivanovskaya *et al.*, 1989).
* – studied in Drits *et al.*, 1997.

In the modified version of the program, the "improvement" stage preset the number of groups of local cation arrangements according to the number of Fe^{3+}-doublets with resolved Δ_j values in the fitted Mössbauer spectrum. Each of these groups represents a combination of arrangements with similar Δ_i^{pred} values. The total occurrence probabilities, W_j, for the groups summed over the individual occurrence probabilities, w_i, for the arrangements belonging to a certain group are compared with the corresponding doublet areas S_j. The derived CD corresponds to the minimum of the function F which should not exceed 0.05:

$$F = \Sigma_j (W_j - S_j)^2 p_j ,$$

where p_j is the penalty for the group j. The "improvement" stage is conducted using a specified number of rearrangements for the ***b***-oriented cation pairs (usually 50000) followed by a specified number of Monte-Carlo runs (usually 100). The total number of cations involved into simulation procedure is equal to 1150 cations, whilst 142 of them are Monte-Carlo updated border and 1008 are working. Function F can act both independently and in combination with "diagonal limitations". Unlike the first version of the program, "diagonal limitations" are applied to all cation pairs oriented along $\boldsymbol{b_1}$ and $\boldsymbol{b_2}$ directions, and not just to $Fe^{3+}Al$ and $R^{2+}R^{2+}$.

The new version of the program applies "diagonal limitations" and the F-function to the analysis of the local cation arrangements around Fe^{2+} as well as those around Fe^{3+}. These calculations can be performed in parallel but independently for Fe^{3+} and Fe^{2+}. The use of the F-function for Fe^{2+} requires knowledge of the individual Δ_i values for Fe^{2+} in the various structural environments. However, neither the Δ_i values nor their assignments are known precisely for Fe^{2+} in these environments. Therefore, interpretations of the Fe^{2+} quadrupole doublets in terms of the local structure in the mineral are made by comparing the occurrence probabilities for the individual cation arrangements around Fe^{2+} with the chemical composition and the S_j and Δ_j values for Fe^{2+} from the Mössbauer spectra.

Table 3. The sums of the occurrence probabilities w_{ik} and w_{ki} (i,k = Al, Fe^{3+}, Fe^{2+} and Mg) for the cationic pairs oriented along the ***b*** axis, by Besson & Drits (1997b).

Sample	69g	68/69	e8/2	40/7	Ch	B.Pat.	136	60
Cation pair								
$Fe^{3+}Fe^{3+}$	0.223	0.181	0.253	0.203	0.126	0.123	0.048	0.014
$Fe^{2+}Fe^{3+}$	0.258	0.19	0.053	0.073		0.010	0.003	
$AlFe^{3+}$	0.056	0.174	0.102	0.087	0.316	0.13	0.091	0.038
$MgFe^{3+}$	0.324	0.188	0.050			0.036		
$Fe^{2+}Fe^{2+}$	0.055					0.017		
$AlFe^{2+}$			0.083	0.108	0.078	0.076	0.131	0.082
$MgFe^{2+}$	0.016		0.043	0.024		0.004	0.034	
AlAl		0.131	0.212	0.278	0.215	0.371	0.256	0.453
MgAl	0.024	0.088	0.13	0.167	0.258	0.206	0.302	0.376
MgMg	0.044	0.048	0.073	0.06	0.008	0.028	0.135	0.036

In order to be acceptable the simulated two-dimensional CDs should satisfy the following criteria:

1. The probability to get minimum of the function F should be 1.0;

2. The statistically weighted Δ_j^{calc} values should be close to the Δ_j values for Fe from computer fits to the spectra;

3. The distribution of the simulated individual occurrence probabilities, w_i for the local cation arrangements as a function of their Δ_i^{pred} values should match qualitatively the form and visual parameters of the spectrum under consideration;

4. The simulated "fine structure" for any given doublet, *i.e.* the corresponding set of w_i and Δ_i^{pred} values, should produce the same line shape as that derived from the Mössbauer spectrum. This problem is discussed in more detail in paragraph 6.1.1.

4. Sample descriptions

Celadonite 69g, glauconites e8/2 and 40/7, illites Ch and 60, and leucophillite 136 with Fe^{3+} contents of 1.46 to 0.17 atoms per crystal-chemical formula and with Fe^{3+}/Fe^{2+} ratios in the range 8.0 to 0.8 were selected for this investigation. In addition, two further samples (glauconites 68/69 and Fe-illite B.Pat.), which had been studied in detail previously (Drits *et al.*, 1997; Dainyak *et al.*, 1984b, 1992), were included in this investigation. These were used to confirm that the new program was able to reproduce the CD reported by Drits *et al.* (1997) and to provide additional data on variations of Fe^{2+} Δ_j values with mineral composition.

The chemical compositions of the samples are presented in Table 2; Fe^{3+}/Fe^{2+} ratios derived from Mössbauer spectra (room temperature) were used in the final calculation of the formulae. In each case, X-ray and oblique texture electron diffraction methods showed that the samples are monomi-

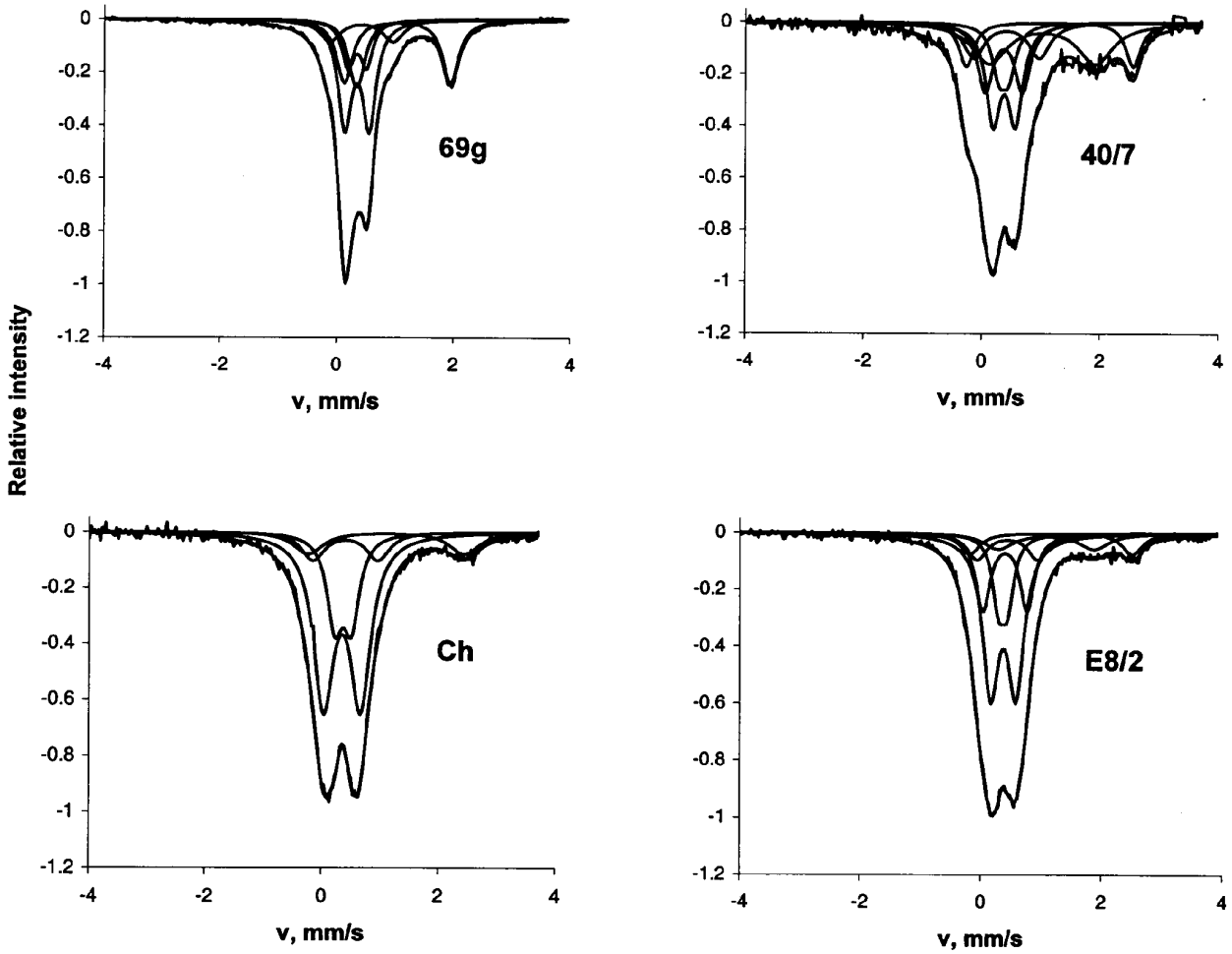

Fig. 2. Fits to the RT Mössbauer spectra, using the approach of Lorentzian-line doublets, of samples 69g, e8/2, 40/7, and Ch.

neralic, belong to 1M or $1M_d$ polytypes, and have vacant trans-sites in their 2:1 layers (Dainyak *et al.*, 1981; Sakharov *et al.*, 1990; Muller *et al.*, 2000). Vacancy of the trans-octahedron may be a characteristic feature of Fe-rich dioctahedral 2:1 layer silicates because the structural studies of these minerals show that they are always trans-vacant (*e.g.*, Tsipursky *et al.*, 1985; Drits *et al.*, 1984; Sakharov *et al.*, 1990; Manceau *et al.*, 1998, 2001; Cuadros 2002; *etc.*).

The IR spectra of all of these samples have been studied in detail by Besson & Drits (1997 a and b). However, because the integrated optical densities of the bands corresponding to the i and k type cations bound to OH groups are used as the initial parameters in the CD simulation, these data are reproduced in Table 3.

5. Experimental: measurement and fitting of Mössbauer spectra

Mössbauer spectra of samples 69g, e8/2, 40/7 and Ch were measured at ambient temperature (RT) on a SM 22001 spectrometer with a constant acceleration drive using a ^{57}Co(Cr) source (experimental half-width $\Gamma = 0.21$ mm/s with a thin Fe foil). The spectra of samples 60 and 136 were measured using a ^{57}Co(Rh) source ($\Gamma = 0.19$ mm/s) on a similar constant acceleration spectrometer by V.S. Rusakov at Moscow State University, Department of Physics. All spectra were calibrated with reference to α-Fe. To eliminate orientation effects, samples were prepared in a hollow cone form with approximately 55° half-cone angle using paraffinium as a holder (Popov *et al.*, 1988). The absorber thickness did not exceed 5–7 mg Fe cm^{-2} with the absorber in the inclined position.

The spectra from samples 69g, e8/2, 40/7 and Ch were fitted to doublets with equal intensities and halfwidths and Lorentzian line shapes (Dainyak, 1980), whereas fits to the spectra from samples 60 and 136 were obtained with a program which used a pseudo-Voigt line shape (Rusakov & Chistyakova, 1992; Rusakov, 2000). There was no specific reason to choose one or other of the fitting models, but the comparison of Lorentzian and pseudo-Voigt line shapes was included into the tests for conformity of simulated two-dimensional CDs to fitted Mössbauer parameters (Section 3). The result of the comparison is discussed in Sections 6.1.1, 6.2.3, and 7.2.

The initial number of doublets used in fits was determined by visual inspection, taking account of any spectral features. As the fitting of Mössbauer spectra is not a precise

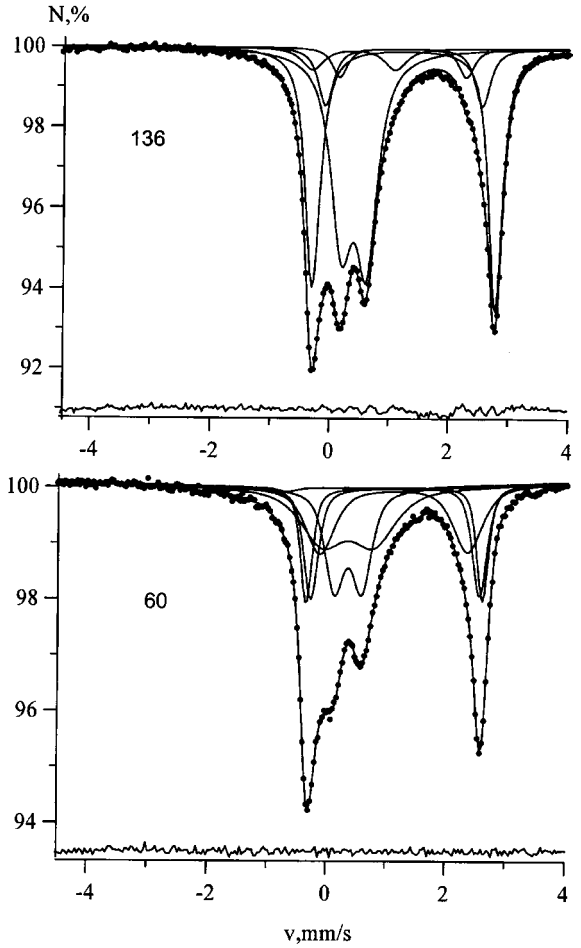

Fig. 3. Pseudo-Voigt-based fits to the RT Mössbauer spectra of samples 136 and 60.

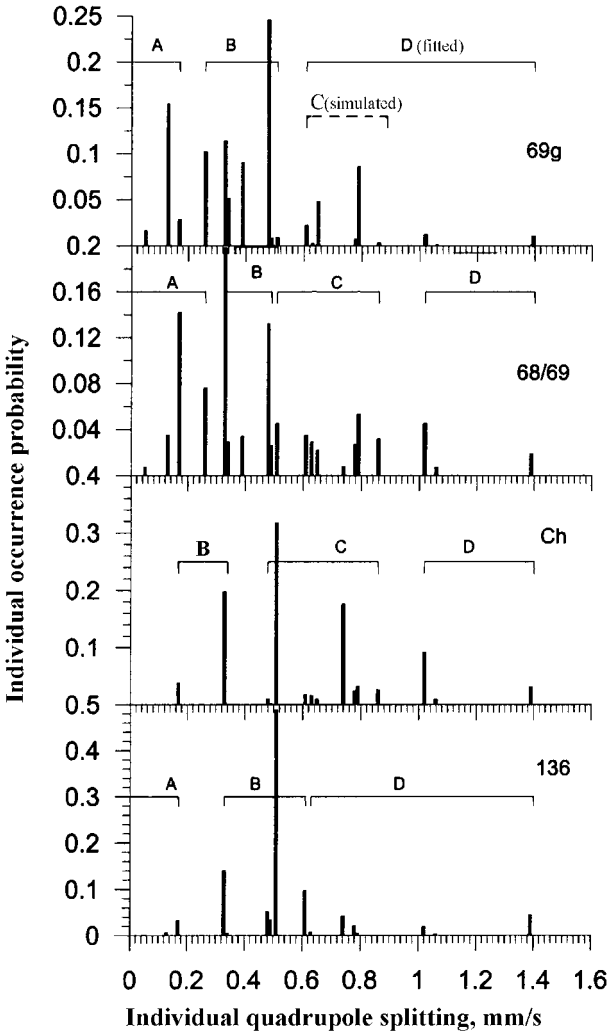

Fig. 4. Simulated individual occurrence probabilities, w_i, as a function of the corresponding predicted Δ_i^{pred} values for the base CD simulation, that is, for the grouping of the local cationic arrangements around Fe^{3+}. Horizontal brackets indicate the grouping by the Δ_i^{pred} values. For sample 69, solid line and dashed line brackets indicate the intensity distributions expected and actually present in accordance with the correspondent Δ_D^{fit} and CD model, respectively.

mathematical problem, the final number of fitted doublets was chosen, not only by the acceptability of χ^2 values, but also taking into account the distances between components in the fitted spectra and any unjustifiable broadening of the peaks.

According to IR data, the studied samples do not contain Fe^{3+} in the tetrahedral sheets of the 2:1 layers (Besson & Drits, 1997 b). Therefore, doublets for Fe^{3+} in tetrahedron were not included into fitting procedure.

6. Results and interpretation

The RT Mössbauer spectra are presented in Fig. 2 and 3, and the parameters from their fits in Table 4. Each spectrum was fitted with 2–4 Fe^{3+} doublets and 1–3 Fe^{2+} doublets. Each Fe^{3+} doublet is defined by a specific range of Δ_j values: 0.09–0.19 mm/s, 0.28–0.46 mm/s, 0.60–0.86 mm/s, and 1.03–1.21 mm/s, denoted by A, B, C, and D, respectively.

The octahedral Fe^{2+} content of dioctahedral phyllosilicates is usually much smaller than this of Fe^{3+}. Thus its contributions to Mössbauer spectra is generally of low intensity (see, for example, the review by Heller-Kallai & Rozenson, 1981). The unusually low Fe^{3+}/Fe^{2+} ratios in samples 136 and 60 (Table 2) result in the presence of intense Fe^{2+} doublets in their Mössbauer spectra (Fig. 3). These spectra were fitted with three quadrupole components Fe^{2+} (Table 4). One Fe^{2+} doublet was fitted to spectra of 69g and Ch, and two Fe^{2+} to the spectra 68/69, e8/2, 40/7 and B.Pat. (Table 4), where the Fe^{2+} content is much lower.

The relative areas of the individual components, S_j, are normalized separately for Fe^{3+} and Fe^{2+} (Table 4), for convenience of use in the CD simulations.

6.1. CD simulation and interpretation of Fe^{3+}-doublets

The initial CD simulation using the IR data of Table 3 was performed with respect to Fe^{3+}, and is referred to as the base simulation. Two limiting cases were considered: (i) the R^{2+} and R^{3+} octahedral cations have equal probability for occupancy of sites M2 and M2', and (ii) the R^{2+} cations have a

Table 4. Mössbauer parameters for the studied samples[1].

Sample and octahedral content	Doublet	Fe^{3+} δ	Fe^{3+} Δ_j	Fe^{3+} Γ	Fe^{3+} S^{norm}	Fe^{2+} δ	Fe^{2+} Δ_j	Fe^{2+} Γ	Fe^{2+} S^{norm}	χ^2
69g	A	0.37	0.12	0.26	0.20	1.07	1.82	0.32	1.	
$Al_{0.08}Fe^{3+}_{1.08}Fe^{2+}_{0.38}Mg_{0.45}$	B	0.37	0.39	0.27	0.62					
	C									
	D	0.41	1.03	0.47	0.18					1.37
69/69*	A	0.34	0.16	0.29	0.26	1.14	2.54	0.31	0.25	
$Al_{0.52}Fe^{3+}_{0.91}Fe^{2+}_{0.19}Mg_{0.37}$	B	0.34	0.42	0.29	0.42	1.05	1.74	0.75	0.75	
	C	0.34	0.72	0.29	0.25					
	D	0.34	1.21	0.29	0.07					1.16
e8/2	A	0.37	0.15	0.24	0.15	1.19	2.61	0.40	0.63	
$Al_{0.66}Fe^{3+}_{0.79}Fe^{2+}_{0.10}Mg_{0.43}$	B	0.37	0.41	0.32	0.52	1.08	1.61	0.59	0.37	
	C	0.36	0.72	0.30	0.22					
	D	0.39	1.03	0.40	0.11					1.16
40/7	A	0.35	0.16	0.27	0.20	1.14	2.80	0.30	0.35	
$Al_{0.87}Fe^{3+}_{0.64}Fe^{2+}_{0.20}Mg_{0.29}$	B	0.37	0.37	0.29	0.32	1.02	1.78	0.73	0.65	
	C	0.37	0.63	0.32	0.31					
	D	0.40	1.10	0.41	0.17					1.12
Ch	A					1.11	2.67	0.61	1.	
$Al_{0.92}Fe^{3+}_{0.74}Fe^{2+}_{0.07}Mg_{0.27}$	B	0.37	0.28	0.38	0.24					
	C	0.36	0.63	0.42	0.63					
	D	0.40	1.17	0.48	0.13					1.33
B.Pat*	A	0.37	0.19	0.28	0.11	1.14	2.82	0.30	0.40	
$Al_{1.11}Fe^{3+}_{0.42}Fe^{2+}_{0.12}Mg_{0.35}$	B	0.37	0.39	0.38	0.59	1.07	1.92	0.57	0.60	
	C	0.37	0.60	0.38	0.25					
	D	0.40	1.08	0.40	0.05					1.10
136	A	0.45	0.11	0.22	0.05	1.11	2.86	0.26	0.70	
$Al_{1.05}Fe^{3+}_{0.17}Fe^{2+}_{0.21}Mg_{0.59}$	B	0.39	0.41	0.37	0.82	1.09	2.44	0.39	0.20	
	C					1.08	1.77	0.55	0.10	
	D	0.46	1.05	0.48	0.13					1.20
60	A					1.13	2.96	0.24	0.28	
$Al_{1.41}Fe^{3+}_{0.10}Fe^{2+}_{0.07}Mg_{0.42}$	B	0.35	0.46	0.39	0.45	1.14	2.84	0.30	0.33	
	C	0.35	0.86	0.87	0.55	1.12	2.49	0.58	0.39	
	D									1.07

[1] δ, Δ, Γ are isomer shift *vs* α-Fe, quadrupole splitting and full width at half-maximum, respectively, all in mm/s; S^{norm} – normalized areas under doublet pikes.

preference for one of the sites. It follows from Table 1 that the individual Δ_i^{pred} values for the local cation arrangements around Fe^{3+} may be conventionally grouped into four groups, each of which combines Δ_i^{pred} values corresponding to one of the four ranges for the fitted Δ_j^{fit} values. The content of these pre-set groups was adjusted so as "manoeuvre" the CD model to fit the Mössbauer parameters. Two or three runs of the program were sufficient to obtain the required CD for all of the samples except 136, which has high Mg content (Table 2). With this sample it was necessary to use the "diagonal limitations" for the MgMg occurrence probability in the b_1- and b_2-directions (Fig. 1), otherwise large Mg-clusters were formed in the CD patterns, which disturbs strongly the homogeneous dispersion of charge.

The results of the simulated CD are shown in Table 5. The total occurrence probabilities W_A, W_B, W_C and W_D of the groups A, B, C and D summed over the simulated individual occurrence probabilities, w_i, are equal to the corresponding doublet areas S_A, S_B, S_C and S_D when the probability to reach minimum of function F is equal to 1.0. The statistically weighted quadrupole splittings, Δ_j^{calc} (j = A, B, C and D), calculated as the sums of the products of the normalized occurrence probabilities, w_i^{norm}, and predicted individual quadrupole splittings, Δ_i^{pred}, for the local arrangements belonging to the group ($\Delta_j^{calc} = \Sigma_i w_i^{norm} \Delta_i^{pred}$) are close to the corresponding Δ_j^{fit} values from computer fits to the spectra. The overstated Δ_D fitted to the spectrum of celadonite 69g may be supposedly referred to the partial Fe^{2+} oxidation during the preparation of the absorber (Bagin *et al.*, 1980). As a matter of fact, the correspondent Δ^{calc} should be referred to the C group.

6.1.1. Distribution of w_i values for corresponding Δ_i^{pred} values, and analysis of the spectral line shapes

The simulated occurrence probabilities, w_i, for the individual Δ_i^{pred} values corresponding to the particular cation arrangements around Fe^{3+} in the simulated CDs are shown in Fig. 4 and 5a. The w_i values are combined into A, B, C and D groups. These distributions appear to conform qualita-

Table 5. Comparison of the total occurrence probabilities, W_j, for the groups and statistically weighted quadrupole splittings, Δ_j^{calc}, with the relative doublet areas, S_j^{norm}, and quadrupole splittings, Δ_j^{fit}, from computer fits to the spectra, respectively.

Sample	j	W_j	S_j^{norm}	Δ_j^{calc}, 1	mm/s 2	Δ_j^{fit}
69g	A	0.198	0.20	0.12		0.12
	B	0.62	0.62	0.39		0.39
	D	0.182	0.18	0.75		1.03
68/69	A	0.26	0.26	0.18	0.19	0.16
	B	0.419	0.42	0.39	0.39	0.42
	C	0.251	0.25	0.69	0.69	0.72
	D	0.071	0.07	1.13	1.13	1.21
e8/2	A	0.146	0.15	0.16	0.16	0.15
	B	0.516	0.52	0.37	0.41	0.41
	C	0.224	0.22	0.73	0.73	0.72
	D	0.114	0.11	1.11	1.03	1.03
40/7	A	0.197	0.20	0.16	0.15	0.16
	B	0.316	0.32	0.33	0.33	0.37
	C	0.314	0.31	0.55	0.63	0.63
	D	0.172	0.17	0.92	1.08	1.10
Ch	B	0.238	0.24	0.30		0.28
	C	0.631	0.63	0.62		0.63
	D	0.132	0.13	1.11		1.17
B.Pat	A	0.108	0.11	0.19	0.18	0.19
	B	0.583	0.59	0.44	0.40	0.39
	C	0.257	0.25	0.68	0.65	0.60
	D	0.047	0.05	1.17	1.11	1.08
136	A	0.041	0.05	0.16	0.11	0.11
	B	0.824	0.82	0.48		0.41
	D	0.142	0.13	0.99		1.05
60	B	0.451	0.45	0.50	0.49	0.46
	C	0.547	0.55	1.06	0.96	0.86

Key: 1 – base CD simulation corresponding to the grouping of the local cation arrangements around Fe^{3+}; 2 – base CD simulation complemented with the grouping of the arrangements around Fe^{2+}.

tively to the corresponding Mössbauer spectra. However, several points may be tested quantitatively: (i) the merits of Lorentzian or pseudo-Voigt line shapes for representing the curve obtained within a given group from the sum of the individual lines of Lorentzian shape weighted by their w_i values. Examples of the curves corresponding to different groups of different samples are given in Fig. 6 and 7; hereafter the corresponding curves will be referred as envelope curves; (ii) the difference δ_{CG} between centers of gravity (CG) for the doublet corresponding to the statistically weighted $\Delta_j^{calc} = \Sigma_i\ w_i^{norm}\ \Delta_i^{pred}$ and that of the envelope curve; (iii) the correlation between full width at half-maximum (halfwidth) of this curve (Γ^{model}) and the corresponding line fitted to the Mössbauer spectrum (Γ^{fit}).

Three groups of the simulated w_i values for different samples will be analyzed in details: the w_i distributions in group B of sample e8/2 (Fig. 5a), group C of sample Ch (Fig. 4), and group C of sample 60 (Fig. 5a). In the first two cases the distributions are slightly asymmetric with narrow and wider velocity ranges, respectively. In the last case, the w_i distribution has a wide velocity range and suggests that the spectrum should be fitted to three Fe^{3+} doublets rather than the two-doublet model presented in Table 4. For each of these groups, analyses were made on sums of Lorentzian lines with the predicted Δ_i^{pred} values, fixed halfwidths, Γ, of 0.28 mm/s and intensities, w_i. These results are shown in Table 6 along with the local cation arrangements around the Fe^{3+} and the positions, x_i, of the corresponding individual Lorentzian lines.

The envelope curves obtained from the weighted sums of the individual Lorentzian lines were approximated by Lorentzian lines. The results of this approximation are presented in Table 6 and also in Fig. 6a for sample e8/2 and Fig. 7a for sample 60. The R values are very good for the narrow velocity ranges of 0.125 mm/s and 0.190 mm/s for samples e8/2 and Ch, respectively. With the wider velocity range in sample 60 (0.395 mm/s), the envelope curve shows two maxima (Fig. 7a). Although this curve can still be approximated by a Lorentzian line, R is 20%. Fitting the envelope curve with a pseudo-Voigt line having Lorentzian and Gaussian components in the same proportion as for the lines fitted to Mössbauer spectrum (Fig. 7b) decreased R to 15 %.

The differences δ_{CG} between CGs for Δ_j^{calc} and the doublet formed by both Lorentzian and pseudo-Voigt line approximations were negligible in each case, and justifies the calculation of model quadrupole splittings Δ_j^{calc} as statistically weighted values using the predicted individual Δ_i^{pred} values (Table 1) and normalized occurrence probabilities w_i^{norm}.

The choice of 0.28 mm/s as the value for Γ for the individual Lorentzian lines was made without any specific reason other than that it represents a reasonable level of broadening over that of the α-Fe standard. The problem of spectral broadening is a complex one and is not addressed in this paper. However, the Γ^{model} values for the envelope curves correlate well with the Γ values obtained from fits to the corresponding Mössbauer spectra (Table 6).

6.2. CD simulation and interpretation of Fe^{2+} doublets

Quadrupole splitting Fe^{2+} is dependent on the octahedral Al and Fe contents, the spectra of the mineral with the highest Al content displaying the largest Δ_j^{fit} values to fit them (Table 4). The predicted individual Δ_i^{pred} values for Fe^{3+} (Table 1) show a similar behavior with the smaller Δ_i^{pred} values corresponding to Fe-rich arrangements and the larger Δ_i^{pred} values to Al-rich arrangements. It seems reasonable to assume, therefore, that the dependence of Δ_i^{pred} values on local cation arrangements is similar for Fe^{3+} and Fe^{2+}. This is referred to below as the postulated sequence.

6.2.1. Individual Δ_i values for Fe^{2+}

The individual occurrence probabilities extracted from the base CD models, w_i, for the postulated sequence of local cat-

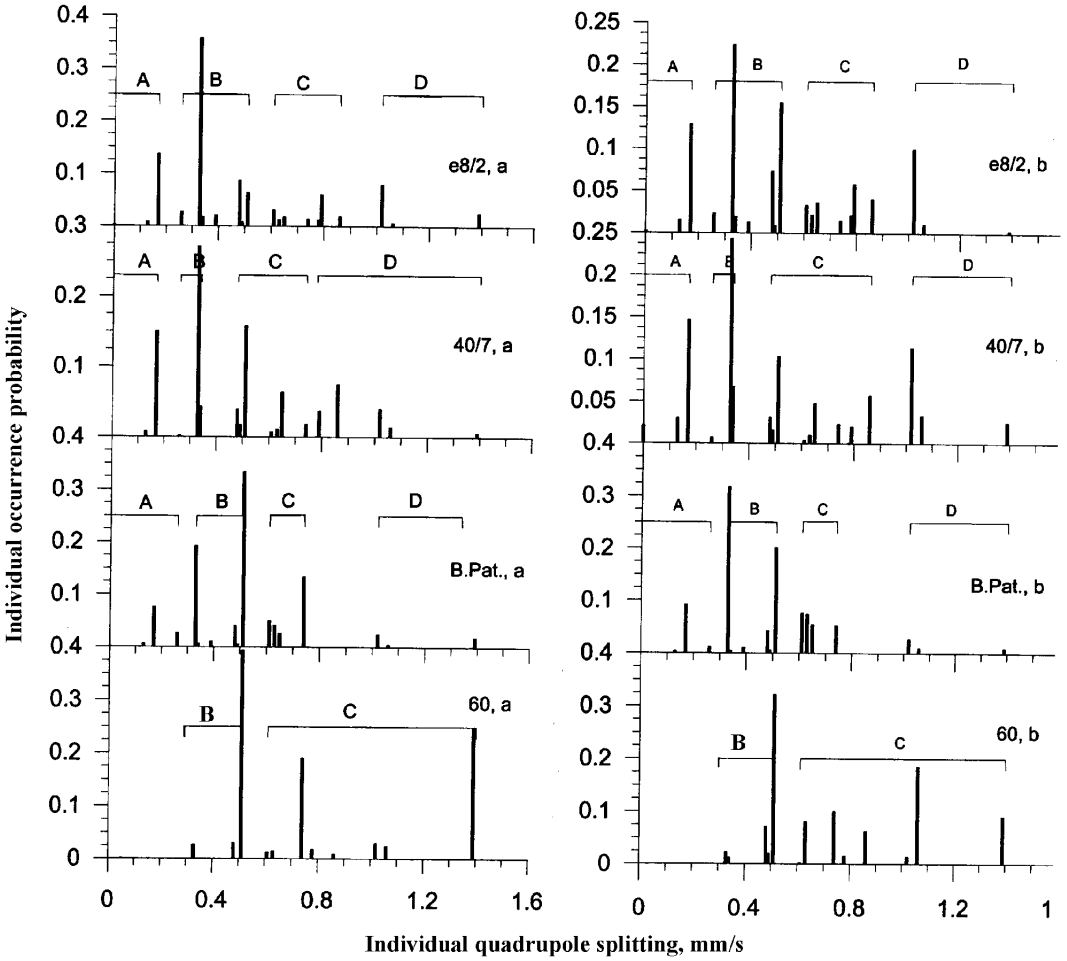

Fig. 5. Simulated individual occurrence probabilities, w_i, as a function of the corresponding predicted Δ_i^{pred} values a) for the base CD simulation when only the local cationic arrangements around Fe^{3+} were grouped, and b) for the base CD simulation complemented with the grouping of the arrangements around Fe^{2+}. Horizontal brackets indicate the grouping by the Δ_i^{pred} values.

ion arrangements around Fe^{2+} are presented in Table 7, where the samples are arranged in order of increasing Al- or decreasing Fe-content (*i.e.* as in Table 4). In the most Fe-rich sample 69g, the maximum occurrence probability of 0.648 belongs to the arrangement $3Fe^{3+}$, whereas for the most Al-rich sample 60, the maximum occurrence probability of 0.702 belongs to the 3Al arrangement. These w_i values correlate with smallest (1.82 mm/s) and largest (2.96 mm/s) Δ_j^{fit} values for Fe^{2+} from fits to the Mössbauer spectra of samples 69g and 60, respectively (Table 4). For other Al-rich samples (B.Pat. and 136), the largest w_i also belong to Al or Al-rich local cation arrangements. Thus, the $2AlFe^{3+}$, 3Al and $2AlFe^{2+}$ local cation arrangements have w_i of 0.27, 0.26 and 0.118, respectively in the base simulation model for sample B.Pat. In sample 136, the 3Al and 2AlMg arrangements have w_i values of 0.276 and 0.326, respectively. Correspondingly, the Mössbauer spectra of these minerals are characterized by rather large Fe^{2+} Δ_j^{fit} values (Table 4). With increasing heterogeneity in the octahedral cation composition, the w_i distributions are characterized by several maxima which correspond to the arrangements from the middle region of the postulated sequence. For example, sample 68/69 has w_i values of 0.486 and 0.373 for the $3Fe^{3+}$ and $2Fe^{3+}Al$ arrangements, respectively, and sample 40/7 has w_i values of 0.158, 0.298, 0.133 and 0.148 for the $2Fe^{3+}Al$, $2AlFe^{3+}$, 3Al and $AlMgFe^{3+}$ arrangements, respectively.

Under these conditions, it is possible to search the relationships between known Fe^{2+} Δ_j^{fit} and w_i values and unknown individual Δ_i values which could be assigned to various local arrangements of Fe^{2+}. This requires examination of different possible groupings of w_i values corresponding to Fe^{2+}. Such groupings should obey the experimental correlations between Δ_j^{fit} and composition of the local cation arrangements around the Fe^{2+}, and should correspond to the postulated sequence for Δ_i and S_j values for fits to Fe^{2+} doublets in the Mössbauer spectra. Finally, they should not have an adverse effect on the base CD models. This last problem is discussed in section 6.2.3.

It is reasonable to start by grouping the Fe^{2+} w_i values for the base CD models in accordance with the numbers of fitted Fe^{2+} quadrupole doublets and taking account of S_j^{fit} values. Such grouping is obvious for samples 68/69, E8/2, 136 and 60, and is shown in columns "1" of Table 7 with underlines. Some groups contain a limited number of statistically meaningful w_i values, which should, therefore, yield simple

Table 6. Local cation arrangements around Fe^{3+} with their simulated w_i values in group B for sample e8/2, in group C for sample Ch and in group C for sample 60, and positions x_i of corresponding individual Lorentzian lines at the velocity scale.*

Arrangement	e8/2			Ch		60		
	x_i mm/s	w_i 1	w_i 2	x_i mm/s	w_i 1	x_i mm/s	w_i 1	w_i 2
$2MgFe^{2+}$	1.100	0.027	0.021					
$2Fe^{3+}Al$	1.135	0.358	0.236					
$2Fe^{2+}Fe^{3+}$	1.140	0.017	0.017					
$3Mg$	1.165	0.020	0.016					
$MgFe^{2+}Fe^{3+}$	1.210	0.087	0.065	1.100	0.010			
$2Fe^{2+}Al$	1.215	0.008	0.007	1.105	0.002			
$2AlFe^{3+}$	1.225	0.063	0.155	1.115	0.317			
$2MgFe^{3+}$				1.165	0.018	1.100	0.012	0.002
$AlMgFe^{2+}$				1.175	0.016	1.110	0.015	0.081
$2Fe^{3+}Fe^{2+}$				1.185	0.010			
$3Al$				1.230	0.176	1.165	0.191	0.100
$2MgAl$				1.250	0.024	1.185	0.018	0.015
$2Fe^{3+}Mg$				1.290	0.032			
$AlFe^{2+}Fe^{3+}$						1.225	0.009	0.063
$AlMgFe^{3+}$						1.305	0.030	0.014
$2AlFe^{2+}$						1.325	0.024	0.185
$2AlMg$						1.495	0.248	0.091
δ_{CG} mm/s Lorentzian		0.001	0.002		0.003		0.003	0.002
δ_{CG} mm/s Pseudo Voigt		–	–		–		0.003	0.007
R(%) Lorentzian		1.7	2.3		4.4		20.3	9.2
R(%) Pseudo Voigt		–	–		–		14.9	4.1
Γ^{model} mm/s Lorentzian		0.30	0.31		0.33		0.55	0.43
Γ^{model} mm/s Pseudo Voigt		–	–		–		0.61	0.49
Γ^{fit}, mm/s		0.32		0.42		0.87		

* R is the factor R for the approximating Lorentzian and pseudo Voigt lines; δ_{CG} is the difference between centers of gravity for the doublet corresponding to statistically weighted Δ_j^{calc} and for the doublet formed by approximating Lorentzian and pseudo Voigt lines; Γ^{model} is the half-width for approximating Lorentzian and pseudo Voigt lines; and Γ^{fit} is the half-width from fits to the spectra; 1 – base CD simulation; 2 – base CD simulation complemented with the grouping of the arrangements around Fe^{2+}.

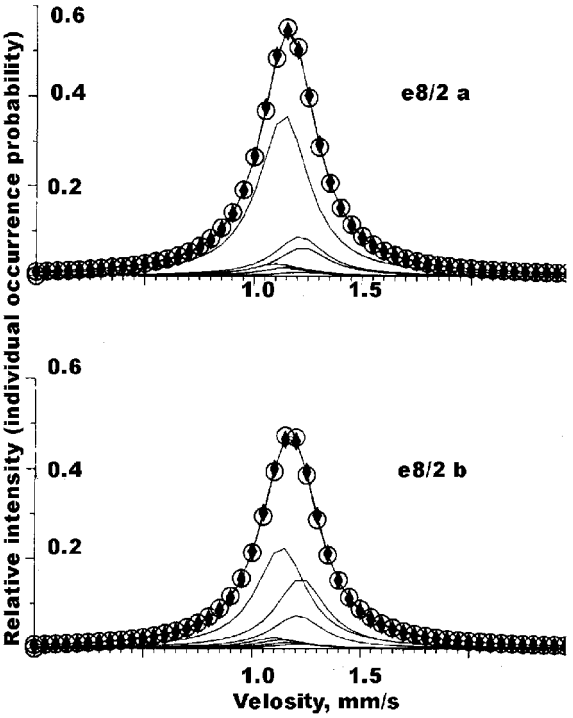

Fig. 6. The envelope curve for the individual Lorentzian-lines constituting the component of the doublet B in the fitted Mössbauer spectrum for sample e8/2 (black rhombuses) and it's approximation by the Lorentzian-line (open circles): a) for the base CD simulation (factor R = 1.7 %); b) for the base CD simulation complemented with the preset grouping of the arrangements around Fe^{2+} (factor R = 2.3 %).

relationships between the Δ_j^{fit} from spectral fits and the individual Δ_i values. At the bottom of Table 7, the relative areas, S_j^{fit}, for Fe^{2+} doublets from spectral fits (Table 4) are compared with the total occurrence probabilities, W_j, summed over the individual w_i values for groups of cation arrangements around Fe^{2+}. This approach was problematic for samples 40/7 and B.Pat., because of the large number of statistically meaningful w_i values, and was inappropriate for samples 69 and Ch because only one doublet was resolved in their spectra.

Let us now analyze these results in more detail. First of all, the distributions of w_i inside the groups follow the experimental correlations between Δ_j^{fit} and composition of local arrangements. For example, the first group for sample 68/69 includes arrangements $3Fe^{3+}$ and $2Fe^{3+}Al$ with maximum w_i values correlating with corresponding low Δ_j^{fit} values (Table 4). However, the total occurrence probabilities, W_j, generally differ from the corresponding S_j^{fit} values. This discrepancy is moderate for samples 68/69 and 136, but for the 1st and 2nd groups for sample 60, the discrepancy is dramatic (Table 7). The distribution of w_i values for sample e8/2 provides an example of a latent disagreement, whilst the S_j^{fit} and W_j values appear to agree very well (Table 7). The essence of this disagreement is as following. It is the spectrum e8/2 for which the smallest Δ (1.61 mm/s) is fitted. This value seems to be assigned to the arrangement $2Fe^{3+}Al$ with $w_i = 0.305$ (Table 7). With the other hand, the Fe-rich sample 69g is fitted with only one Fe^{2+} doublet with Δ = 1.82 mm/s, which is supported mainly from the $3Fe^{3+}$ arrangement ($w_i = 0.648$, Table 7). In view of the dependence of Fe^{2+} Δ_i values on the postulated sequence of the arrangements around the Fe^{2+} ion, Δ_i for the $3Fe^{3+}$ arrangement should be smaller then that for the $2Fe^{3+}Al$ arrangement. Therefore, doublet with Δ = 1.61 mm/s should be assigned to $3Fe^{3+}$, whereas the doublet with Δ = 1.82 mm/s most probably corresponds to the $2Fe^{3+}Al$ arrangement. To overcome these disagreements, we have undertaken the additional computer simulation with the preset grouping with respect to Fe^{2+}.

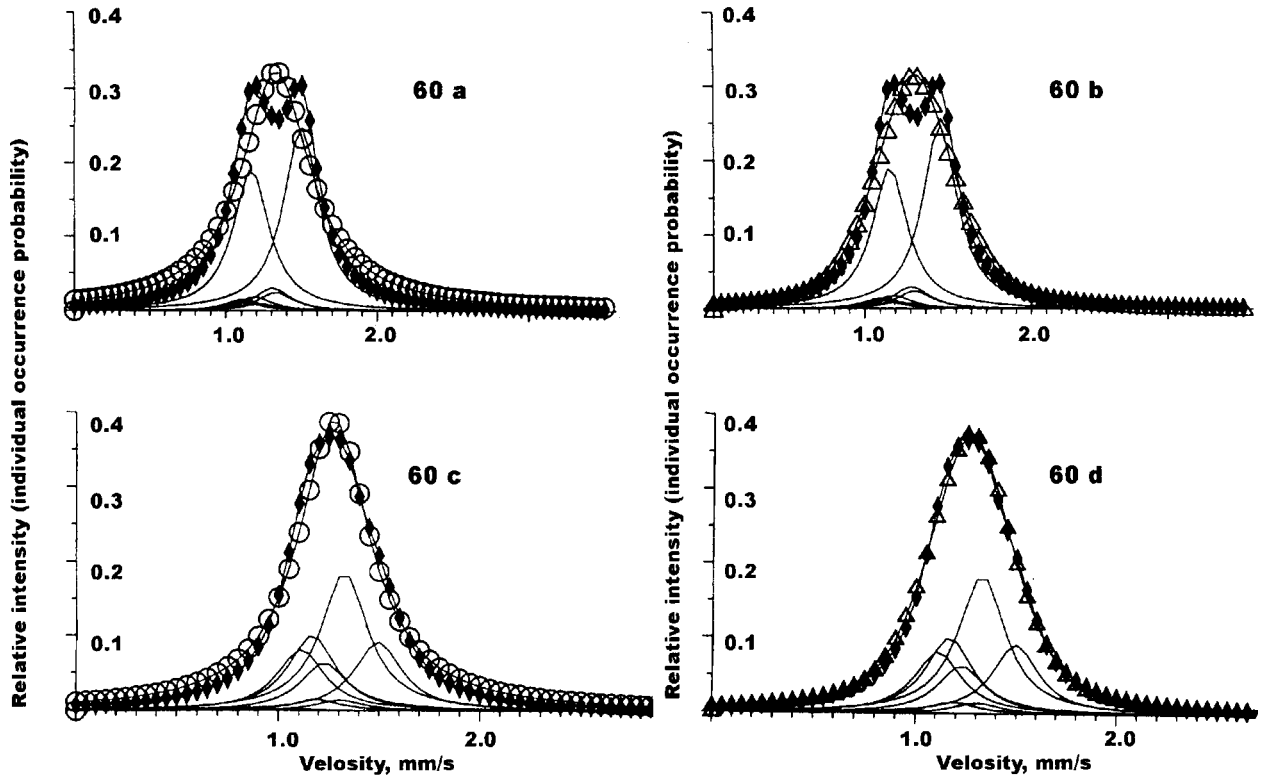

Fig. 7. The envelope curve (black rhombuses) for the individual Lorenzian-lines corresponding to the w_i-distribution in the group C for the base CD simulation for sample 60 and it's approximation (a) by Lorentzian line (R = 20.3 %) and (b) by pseudo Voigt line (R = 9.2 %); and for the additional CD simulation using preset grouping of cationic arrangements around Fe^{2+} and it's approximation (c) by Lorentzian line (R = 14.9 %) and (d) by pseudo Voigt line (R = 4.1 %). Lorentzian- and pseudo-Voigt-approximations are presented with open circles and triangles, respectively.

Introducing control of the preset groupings of cation arrangements around Fe^{2+} by use of function F in the simulation procedure changes the compositions of the groups significantly. The first group for sample e8/2 now contains only the $3Fe^{3+}$ arrangement, which corresponds to the smallest Δ_j^{fit} from the spectral fit. Thus

$$\Delta(3Fe^{3+}) = 1.61 \text{ mm/s}. \quad (1)$$

Each of three groups for sample 60 degenerates into single arrangements, each of which is Al-rich. In view of the dependence of Δ_j^{fit} on the octahedral Al content and the postulated sequence, the following assignments can be derived:

$$\Delta(2AlFe^{3+}) = 2.49 \text{ mm/s} \quad (2)$$

$$\Delta(3Al) = 2.84 \text{ mm/s} \quad (3)$$

$$\Delta(2AlMg) = 2.96 \text{ mm/s}. \quad (4)$$

Better agreement between calculated and experimental results is now found for samples 68/69 and 136. If one neglects small w_i values, simple relationships of a form similar to the Δ_j^{calc} for Fe^{3+} can be derived, *i.e.* $\Delta_j^{calc} = \Sigma_i w_i^{norm} \Delta_i$, whilst the sums $W_j = \Sigma_i w_i$ over the corresponding simulated individual w_i are equal to S_j^{fit} of the corresponding fitted doublets. For sample 68/69:

$$0.44 \cdot \Delta(3Fe^{3+}) + 0.56 \cdot \Delta(2Fe^{3+}Al) = 1.74 \text{ mm/s}. \quad (I)$$

For sample 136:

$$0.4 \cdot \Delta(2MgFe^{2+}) + 0.3 \cdot \Delta(2Fe^{3+}Al) + 0.3 \cdot \Delta(3Mg) = 1.77 \text{ mm/s} \quad (II)$$

$$0.4 \cdot \Delta(3Al) + 0.16 \cdot \Delta(2MgAl) + 0.44 \cdot \Delta(2AlMg) = 2.86 \text{ mm/s}. \quad (III)$$

Substituting (1) into (I) one derives:

$$\Delta(2Fe^{3+}Al) = 1.85 \text{ mm/s}. \quad (5)$$

Estimates of $\Delta(2MgFe^{2+})$ and $\Delta(3Mg)$ in (II) can be obtained using (5) and a trial-and-error approach. This yields the following assignments, which are consistent with the postulated sequence:

$$\Delta(2MgFe^{2+}) = 1.70 \text{ mm/s} \quad (6)$$

$$\Delta(3Mg) = 1.90 \text{ mm/s} \quad (7)$$

Using assignments (3) and (4), relationship (III) is satisfied with:

$$\Delta(2MgAl) = 2.85 \text{ mm/s}. \quad (8)$$

This last value is also consistent with the postulated sequence. Thus, a total of eight individual Δ_i values for different

Table 7. Simulated individual occurrence probabilities, w_i , for the local arrangements around Fe^{2+}.*

Sample	69g	68/69		e8/2		40/7	Ch	B.Pat	136		60	
Arrangement	1	1	2	1	2	1	1	1	1	2	1	2
$3Fe^{2+}$	0.002							0.001				
$2Fe^{2+}Mg$	0.004					0.001		0.008	0.001			
$3Fe^{3+}$	0.648	0.486	0.326	0.075	0.365	0.046		0.006				
$2MgFe^{2+}$	0.006					0.005		0.015	0.015	0.038		
$2Fe^{3+}Al$	0.021	0.373	0.414	0.305	0.001	0.158	0.082	0.081	0.008	0.031		
$2Fe^{2+}Fe^{3+}$	0.054							0.004				
3Mg						0.001		0.001	0.038	0.032		
$MgFe^{2+}Fe^{3+}$	0.131					0.008		0.008	0.002	0.022		
$2Fe^{2+}Al$	0.003							0.021				
$2AlFe^{3+}$		0.066	0.134	0.345	0.358	0.298	0.399	0.270	0.104	0.168	0.048	0.380
$2MgFe^{3+}$	0.015	0.001	0.004	0.002		0.004		0.001	0.011	0.010		
$AlMgFe^{2+}$	0.004							0.055	0.016	0.012	0.002	
$2Fe^{3+}Fe^{2+}$	0.101							0.014				
3Al				0.122	0.158	0.133	0.499	0.260	0.276	0.249	0.702	0.340
2MgAl				0.005	0.004	0.016		0.006	0.125	0.097	0.002	
$2Fe^{3+}Mg$	0.011	0.052	0.101	0.026		0.052		0.003	0.002	0.001		
$AlFe^{2+}Fe^{3+}$	0.001					0.008		0.067	0.002	0.001	0.002	
$AlMgFe^{3+}$		0.022	0.021	0.072	0.059	0.148	0.005	0.024	0.062	0.032	0.010	
$2AlFe^{2+}$						0.007		0.118	0.012	0.013	0.071	0.020
2AlMg				0.048	0.055	0.116	0.014	0.037	0.326	0.273	0.162	0.260
S_j^{norm}	1.	0.75	0.75	0.37	0.37	0.65	1.	0.60	0.10	0.10	0.39	0.39
		0.25	0.25	0.63	0.63	0.35		0.40	0.20	0.20	0.33	0.33
									0.70	0.70	0.28	0.28
W_j	1.	0.86	0.75	0.38	0.37		1.		0.06	0.09	0.05	0.38
		0.14	0.25	0.62	0.63				0.12	0.23	0.70	0.34
									0.82	0.68	0.25	0.28

* (1) – base CD models, (2) base CD models complemented with grouping of the arrangements around Fe^{2+}. The obvious grouping (1) and the grouping controlled by function F (2) are indicated by underlines. The Table also compares the total occurrence probabilities, W_j, for the groups and the relative areas, S_j^{norm}, for the Fe^{2+} doublets from computer fits to the spectra.

Table 8. Individual Δ_i^{tent} values for some local cation arrangements around Fe^{2+}.

Arrangement	$3Fe^{3+}$	$2MgFe^{2+}$	$2Fe^{3+}Al$	3Mg	$2AlFe^{3+}$	3Al	2MgAl	2AlMg
Δ_i^{tent}, mm/s	1.61	1.70	1.85	1.90	2.49	2.84	2.85	2.96

cation arrangements around Fe^{2+} have been derived. These are referred to in Table 8 and below as „tentative", Δ_i^{tent}.

6.2.2.Examination of the individual Δ_i^{tent} values for Fe^{2+}

The eight Δ_i^{tent} values cover almost the entire range of possible quadrupole splittings for Fe^{2+} in different local cation arrangements. It is possible, therefore, to estimate the missing values by analogy with proportions which are characteristic for the Fe^{3+} Δ_i^{pred} values (Table 1). The Δ_i^{tent} values derived in this way are marked in italic in Table 9. Now this complete set of Δ_i^{tent} for Fe^{2+} can be examined using the simulated individual w_i for the second groups of arrangements for samples 68/69, e8/2 and 136, which were not used in the derivation of the original eight Δ_i^{tent} values and for samples 69g, 40/7 and B.Pat. The results are shown in Table 9, which presents details for the calculation of statistically weighted Δ_j^{calc} values for Fe^{2+} and compares them with Δ_j^{fit} values from fits to the Mössbauer spectra. The satisfactory agreement between calculated and fitted quadrupole splittings Fe^{2+} indicates that the Δ_i^{tent} values are reasonable.

6.2.3. CD simulations using the preset grouping of the local cation arrangements around Fe^{2+} and Fe^{3+}

The distribution of the simulated individual w_i for the local cation arrangements around Fe^{3+} as a function of their Δ_i^{pred} values (Table 1) corresponds more closely to the form of the spectra when the preset groupings of the local cation arrangements around Fe^{2+} are incorporated into the calculations (Fig. 5b). This is especially noticeable for sample 60 where the new w_i-distribution (Fig. 5b) shows a close correspondence with the two-Fe^{3+}-doublet fit (Table 4).

The w_i values from this additional CD simulation are presented in Table 6 (columns 2), along with the line shape analyses (Fig. 6b, Fig. 7c,d). The values for R, Γ^{model} and δ_{CG} show virtually no change for the group of individual Lorentzian lines in the narrow velocity (sample e8/2), and the visual improvement in the w_i-distribution (Fig. 5b) is unimportant in this case. In contrast, the new w_i-distribution within group C of sample 60 (Fig. 5b, Table 6 column 2) yields much improved R values for both Lorentzian and pseudo-Voigt line shapes. However, the Γ^{model} for the pseu-

Table 9. Examination of the individual Δ_i^{tent} values for Fe^{2+}.

Arrangement	Δ_i^{tent}	69g		68/69*			e8/2*			40/7			Ch		B.Pat			136		
		w_i	$\Delta_i^{tent}w_i$	w_i	w_i^n	$\Delta_i^{tent}w_i^n$	w_i	w_i^n	$\Delta_i^{tent}w_i^n$	w_i	w_i^n	$\Delta_i^{tent}w_i^n$	w_i	$\Delta_i^{tent}w_i$	w_i	w_i^n	$\Delta_i^{tent}w_i^n$	w_i	w_i^n	$\Delta_i^{tent}w_i^n$
$3Fe^{2+}$	*1.20*	0.002	0.002												0.005	0.008	0.010			
$2Fe^{2+}Mg$	*1.40*	0.004	0.006							0.005	0.008	0.011			0.017	0.028	0.039			
$3Fe^{3+}$	**1.61**	0.648	1.043							0.040	0.063	0.101			0.006	0.010	0.016			
$2MgFe^{2+}$	**1.70**	0.006	0.010							0.020	0.031	0.052			0.022	0.037	0.061			
$2Fe^{3+}Al$	**1.85**	0.021	0.040	____	____	_____	0.001	0.002	0.004	0.522	0.818	1.513	0.082	0.152	0.184	0.309	0.572			
$2Fe^{2+}Fe^{3+}$	*1.87*	0.054	0.105												0.019	0.032	0.060			
3Mg	**1.90**									0.022	0.034	0.065			0.002	0.003	0.006	____	____	_____
$MgFe^{2+}Fe^{3+}$	*2.10*	0.131	0.275							0.027	0.042	0.089			0.077	0.129	0.271	0.022	0.110	0.231
$2Fe^{2+}Al$	*2.30*	0.003	0.007							0.002	0.003	0.007			0.086	0.144	0.331			
$2AlFe^{3+}$	**2.49**			0.134	0.506	1.259	0.358	0.564	1.404	0.092	0.255	0.635	0.399	0.994	0.178	0.298	0.742	0.168	0.840	2.092
$2MgFe^{3+}$	*2.60*	0.015	0.039	0.004	0.015	0.039				0.001	0.003	0.007						0.010	0.005	0.013
$AlMgFe^{2+}$	*2.65*	0.004	0.011							0.002	0.005	0.015			0.026	0.064	0.171			
$2Fe^{3+}Fe^{2+}$	*2.75*	0.101	0.278												0.036	0.089	0.244			
3Al	**2.84**						0.158	0.249	0.707	0.149	0.413	1.172	0.499	1.417	0.164	0.405	1.150			
2MgAl	**2.85**						0.004	0.006	0.017	0.005	0.014	0.039			0.003	0.007	0.021			
$2Fe^{3+}Mg$	*2.87*	0.011	0.032	0.101	0.381	1.093				0.003	0.008	0.023			0.002	0.005	0.014			
$AlFe^{2+}Fe^{3+}$	*2.87*	0.001	0.003							0.006	0.024	0.069			0.038	0.094	0.269			
$AlMgFe^{3+}$	*2.87*			0.021	0.079	0.227	0.059	0.093	0.267	0.030	0.083	0.238	0.005	0.014	0.025	0.062	0.177			
$2AlFe^{2+}$	*2.90*						0.055	0.087	0.261	0.018	0.049	0.145	0.014	0.042	0.072	0.178	0.515			
2AlMg	**2.96**									0.055	0.152	0.457			0.039	0.096	0.289			
Δ_j^{calc} =			1.85			2.62			2.66			1.83		2.62			2.10			2.34
$\Sigma_i\Delta_i^{tent}\,w_i^n$, mm/s												2.80					2.84			
Δ_j^{fit}, mm/s			1.82			2.54			2.61			1.78		2.67			1.92			2.44
												2.80					2.82			

* Calculation for the second group of the simulated individual occurrence probabilities, w_i.

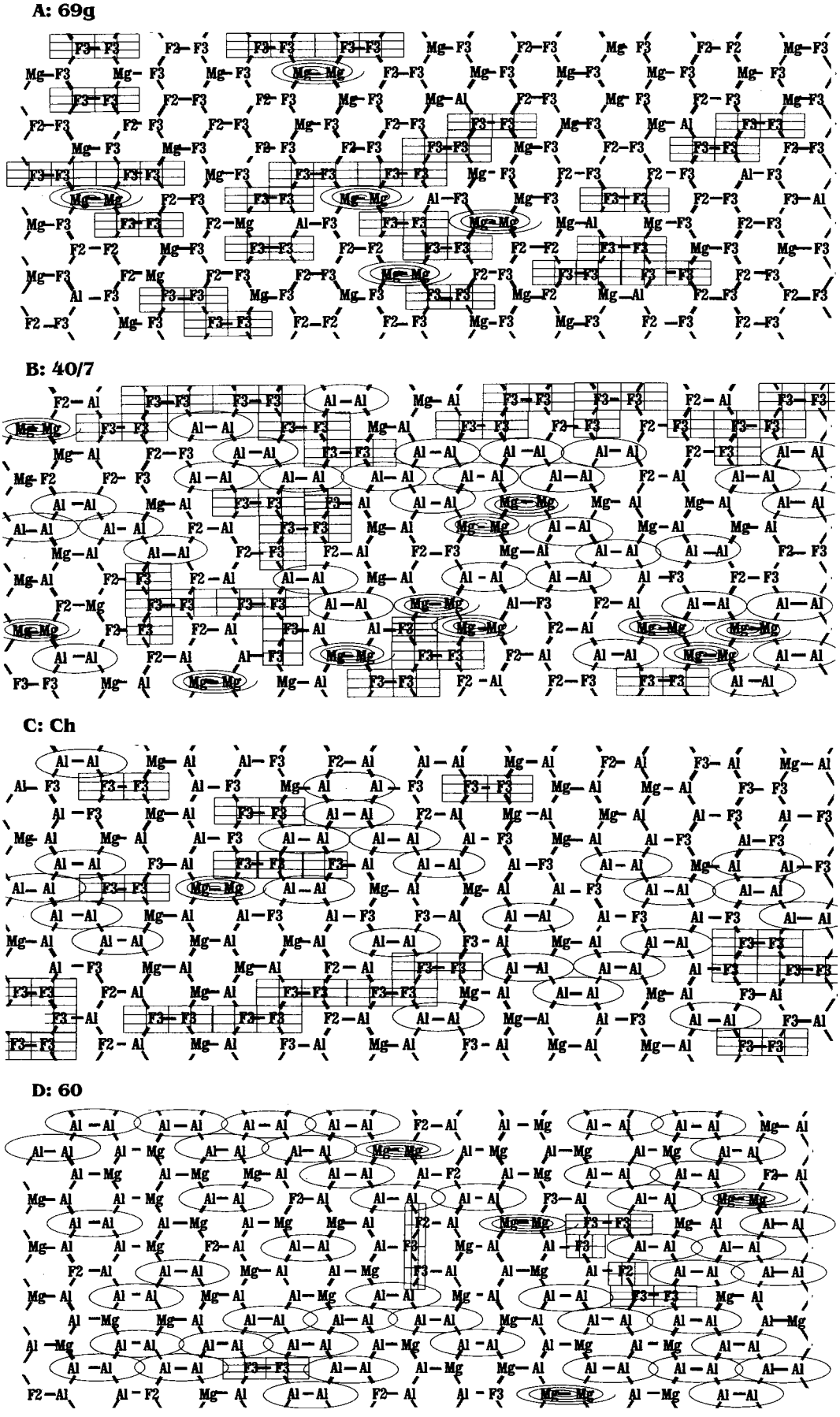

Fig. 8. Patterns of two-dimensional cation distribution derived for samples 69g (a), 40/7 (b), Ch (c), and 60 (d).

do-Voigt line shape is closer to the Γ^{fit} than the Lorentzian line shape (Table 6). In almost every case, the statistically weighted Δ_j^{calc} values produced by the CD simulation controlled both Fe^{3+} and Fe^{2+} (Table 5 column 2) are in better agreement with Δ_j^{fit} values than those from the base simulation.

6.3. Octahedral cation distribution models

Examples for patterns of CDs which satisfy the fitted Mössbauer spectral parameters for the corresponding minerals are shown in Fig. 8. The main features of the CDs for samples 68/69 and B.Pat. obtained with new simulation program are similar to those of Drits *et al.* (1997). With the exception of sample 60, a preference of R^{2+} cations for one of the two symmetrically independent cis-sites is a common feature of the patterns. There is thus a tendency to obey the homogeneous distribution of octahedral cation charge. For sample 60, however, function F in the simulation procedure is minimized when the R^{2+} and R^{3+} octahedral cations are randomly distributed over the two cis-sites.

The CD pattern for celadonite 69g (Fig. 8a) includes Fe^{3+}-clusters of different sizes, and the MgMg, $Fe^{2+}Fe^{2+}$ and $MgFe^{2+}$ pairs tend to be adjacent to Fe^{3+}-clusters. In the greatest cluster of this pattern containing Fe^{2+}, Mg and Fe^{3+} cations, each of R^{2+} cations holds R^{3+} in its closest surrounding and *vice versa* providing the long-range homogeneous dispersion of the octahedral charge.

The clustered structures of glauconites e8/2, 40/7 (Fig. 8b) are very similar. They are characterized by Fe^{3+}-clusters and Al-clusters of moderate size and by small Mg-clusters. The separation into homogeneous clusters is so pronounced that the clusters of mixed cation composition (mainly Mg, Al) are quite small. Similar effects were found in glauconite 68/69 (see Fig. 8c in Drits *et al.*, 1997).

The CD patterns for the ferri-illites Ch, 60 and B.Pat. are more diverse. There are much less Mg segregated pairs (Table 3) than in the glauconites, and the degrees of Al and Fe^{3+} segregation are quite different. For example, Al segregation is the highest in B.Pat. (Fig. 8e in Drits *et al.*, 1997), intermediate in sample 60 (Fig. 8d) and smallest in sample Ch (Fig. 8c). Correspondingly, more large clusters of mixed cation composition are observed in the patterns for samples Ch and 60. These clusters contain Mg, Al, Fe^{3+} and Mg, Al, Fe^{2+} for samples Ch and 60, respectively. It is interesting that, in spite of the lack of any site preference for R^{2+} in sample 60, the clusters of mixed composition are characterized by groupings having R^{3+} cations surrounded by R^{2+} cations and *vice versa* prevailing. It means that R^{2+} cations occupy either M2 or M2' sites in different clusters. It was reported by Coey (1980) that Mössbauer spectra of Fe-illite are characterized by more variable parameters than glauconite spectra. It is evident now that the CD is the reason for this behavior.

The nature of the CDs in octahedral sheets may reflect the conditions under which the minerals were formed. Thus, the globular Fe-illite B.Pat. is characterized by a much higher level of Al and Fe segregation than the finely dispersed Fe-illite Ch, although their overall compositions are similar (Table 2).

The CD of leucophyllite 136 is different from those of the other minerals investigated. In spite of predominance of R^{3+} cations in the octahedral sites (Table 2), visible Mg-segregation is observed, in parallel with pronounced Al segregation and little Fe segregation, even when the CD simulation was constrained to prevent large Mg-segregation (Section 6.1). In addition, dispersion of octahedral charge in the clusters of mixed cation composition (mainly Mg, Al) is rather homogeneous.

7. Discussion

7.1. The individual quadrupole splittings for the local cation arrangements around Fe^{2+}

The first step to interpreting the Fe^{2+} quadrupole doublets from fits to Mössbauer spectra of dioctahedral trans-vacant micas by superposition of individual doublets corresponding to different local cation arrangements has now been accomplished. Based on a combination of the experimental dependence of the Fe^{2+} quadrupole splittings on the composition of a representative collection of well-characterized minerals and their CD simulation results, several individual Fe^{2+} quadrupole splittings have been assigned to specific local cation arrangements (Table 8). These splittings are referred as tentative, Δ_i^{tent}, because the values are probably semi-quantitative ones. They are, however, of practical value, if one takes into account the following considerations.

(i) The set of Δ_i^{tent} values for Fe^{2+} combined with the new CD simulation program (see section 3) provide an additional means for controlling the CD reconstruction. CD models can now be produced to satisfy both the Fe^{3+} and Fe^{2+} Mössbauer spectral parameters. As shown in section 6.2.3, the results of the base CD simulation can be improved significantly by using a function F in the simulation procedure to regulate the individual occurrence probabilities, w_i, of the local arrangements for both Fe^{3+} and Fe^{2+}. In this case, the Fe^{3+} w_i-distributions of the individual Δ_i values correspond more closely to the experimental spectra than those obtained for the base simulation, and the statistically weighted Δ_j^{calc} values are in better agreement with the corresponding Δ_j^{fit} values from spectral fits.

(ii) The consecution of local cation arrangements in terms of increasing quadrupole splitting is the same both for Fe^{3+} and Fe^{2+}, and implies a direct dependence of the Fe^{2+} quadrupole splitting on the structural distortion at Fe^{2+} site. This is an important observation, because the valence and lattice contributions to Fe^{2+} quadrupole splittings are accepted as having opposite signs. Thus, based on the theoretical work of Ingalls (1964), Bancroft (1974) developed the concept that the smallest Δ values correspond to the largest distortions of Fe^{2+} sites in minerals. However, on the basis of the temperature dependence of the spectra of the trioctahedral mica, phlogopite, Huggins (1976) calculated that the splittings of the t_{2g} electronic levels were small enough to produce at room temperature the opposite trend to that predicted by the Ingalls model. Later, on the basis of qualitative estimations of the admixture of excited state orbitals with the ground state wave function, Mineeva (1978) also con-

cluded that the Fe^{2+} doublets with smaller Δ values resulted from smaller values for q_{val}. The results reported in this paper are in agreement with this conclusion.

Bearing in mind that the data of Table 1 and Table 9 represent q_{lat} and $q_{val}+q_{lat}$ respectively, and that q_{val} and q_{lat} have the opposite signs, one can estimate the range of q_{val} as 1.8 – 4.5 mm/s in these room temperature spectra.

The observed dependence of the Fe^{2+} Δ values on the octahedral Al and Fe content is not unique. The increase of Δ_j^{fit} with increasing Al content was observed for Fe-bearing mixed-layer illite-smectites (Lindgreen *et al.*, 1991; Drits *et al.*, 2002). However, the opposite trend was found in Mössbauer spectra of synthesized trioctahedral potassium micas: quadrupole splittings decrease slightly with increasing Al content (Redhammer, 1998; Redhammer *et al.*, 2000, 2002). Thus, the local effects for $F^{2+}\Delta$ values are different for di- and trioctahedral micas.

7.2. The w_i-distribution and line shape

For the predicted individual Δ_i^{pred} values, the distribution of the w_i for the local cation arrangements around Fe^{3+} (section 6.1.1) is analogous to the Quadrupole Splitting Distribution (QSD) analysis developed by Rancourt & Ping (1991). However, unlike QSD analysis, the w_i-distribution has a clear crystal-chemical foundation. As shown in section 6.2.3, even visual evaluation of the conformity of the w_i-distribution to the spectral parameters was sufficient to choose the CD reconstruction with the same number of envelope Lorentzian-line doublets as the corresponding spectrum fitting. Lorentzian lines approximate sets of the simulated w_i values with narrow velocity ranges (0.06 – 0.17 mm/s) with good values for R (~2%), whilst pseudo-Voigt lines may be more appropriate for sets of individual Lorentzian lines spanning wider velocity ranges (~ 0.4 mm/s). This example illustrates the reason for better χ^2 values using pseudo-Voigt-lines.

7.3. Problems with the assignment of Δ_i^{pred} and Δ_i^{tent} values

There is a degree of uncertainty in the assignments of the individual Fe^{3+} and Fe^{2+} quadrupole splittings, Δ_i^{pred} and Δ_i^{tent}, to local cation arrangements. Two possible approaches for increasing the reliability of the assignments are discussed below. The first (theoretical) approach involves direct calculation of the EFGs at the Fe^{3+} and Fe^{2+} sites. Calculations of the lattice contributions to EFG, q_{lat}, are feasible for Fe^{3+}, if accurate atomic coordinates are available for the nearest and next nearest anions and cations (Bookin *et al.*, 1978; Dainyak *et al.*, 1981; 1984 a, b, c). Although q_{lat} values can now be derived using structural modelling methods (Brown & Shannon, 1973; Brown, 1981, 1992; Parker *et al.*, 1984; Brown & Altermatt, 1985; Brese & O'Keefe, 1991; Kroll *et al.*, 1992; Smoliar-Zviagina, 1993; Manceau *et al.*, 1998), there are difficulties in calculating q_{val} contributions to EFGs for Fe^{2+}. The second (experimental) approach involves intensive analysis of high quality experimental data from well-defined mineral specimens in order to refine the assignments.

7.4. Cation distribution models

The diversity of the CDs in the studied minerals may be considered to result from several competitive factors. The most important of them are the predominance of R^{3+} cations in octahedral sheets (Table 2), the presence, in spite of the first factor, of R^{2+}-OH-R^{2+} pairs (Table 3), and the preference of R^{2+} cations for one of the two symmetrically independent cis-sites. The combination of these factors yields clustered structures, that contain R^{3+}- and R^{2+}-clusters, as well as clusters of mixed composition with R^{3+} surrounded by R^{2+} and *vice versa*.

The cluster sizes are not determined by chemical composition directly. Thus, globular and finely dispersed Fe-illites, having approximately the same composition, are characterized by significantly different levels of Al and Fe^{3+} segregation. Another example is Fe segregation observed even in structures with low Fe content. It should be noticed that such a segregation seems to be common in dioctahedral phillosilicates, and significant clustering has been reported for glauconites (Drits *et al.*, 1997) and for bentonitic illite-smectites (Sainz-Diaz *et al.*, 2000, 2001).

Clustered structures are not at variance with Pauling's principle of homogeneous dispersion of charge. This principle is always obeyed in the R^{3+}, R^{2+}-clusters with the strict alternation of R^{3+} and R^{2+} cations over the two symmetrically independent cis-sites. Neither is it disturbed by homogeneous clusters if one takes account of Al for Si substitution in tetrahedra neighbouring with R^{3+}-clusters to optimise the charge compensation.

The results discussed here are the most straightforward ones, but there are still a number of outstanding questions concerning the influence of mineral composition and genesis on the degree of segregation of different types of cations. Our approach, which includes the use of IR-data in addition to structural details determined by diffraction methods, has yielded significant progress in the resolution of such problems by interpreting Mössbauer spectra of micaceous trans-vacant minerals. It also has the potenzial for application to other layer minerals.

7.5. Problems in the CD simulation

One of the main limitations in simulation of CDs is that the mica IR and Mössbauer spectra do not contain information concerning occurrence probabilities for Mg-Mg, Al-Mg and Al-Al cation pairs oriented along the b_1- and b_2-directions. Therefore, uncertainties in simulated CDs especially increase for micas with low content of Fe^{3+} and Fe^{2+}. In particular, probably because of the low content of these cations in sample 136, the simulated CD contains relatively large Mg-clusters violating the Pauling's principle.

Additional difficulties in CD simulation consist in the quantitative measurements of individual OH-bands of low intensities, especially in cases when their positions are overlapped with those for the water molecular bands.

The CD simulation process could benefit from additional data from other techniques, *e.g.* on Al, Si distributions in tetrahedral sheets determined by NMR spectroscopy.

8. Conclusions

Computer simulation of CD models in dioctahedral minerals generates structures, whose detailed compositions satisfy both IR and Mössbauer spectroscopic data in addition to overall structures determined by diffraction methods. A major feature of these models is the development of the concept of clustered structures for these minerals. Building on previous work with Fe^{3+}, the present results provide a major increase in our understanding of the distribution of the chemical environments around Fe^{2+} ions.

Acknowledgments: Authors gratefully acknowledge Dr. B. Goodman for valuable comments, suggestions and the English editing. We also thank Prof. V.S. Rusakov for use of his Mössbauer facility and Drs. Redhammer and Lottermoser for their useful comments and suggestions. This research was supported by the Russian Science Foundation (grant 01–05–64486).

References

Bagin, V.I., Gendler, T.S., Dainyak, L.G., Kuz'min, R.N. (1980): Mössbauer, thermomagnetic, and X-ray study of cation ordering and high-temperature decomposition in biotite. *Clays Clay Minerals*, **28**, 188–196.

Bailey, S.W. (1984): Crystal chemistry of the true micas. *In* Bailey reviews in mineralogy, v. **13.** Micas, 1–12. Mineral. Soc. Am., Chelsea, Mich., USA.

Bancroft, G.M. (1974): Mössbauer spectroscopy. MacGraw Hill, New York, 252 p.

Besson, G. & Drits, V.A. (1997a): Refined relationships between chemical composition of dioctahedral fine-dispersed mica minerals and their infrared spectra in the OH stretching region. Part I: Identification of the stretching bands. *Clays Clay Minerals*, **45**, 158–169.

–, – (1997b): Refined relationship between chemical composition of dioctahedral fine-dispersed mica minerals and their infrared spectra in the OH stretching region. Part II: The main factors affecting OH vibration and quantitative analysis. *Clays Clay Minerals*, **45**, 170–183.

Besson, G., Bookin, A.S., Dainyak, L.G., Rautureau, M., Tsipursky, S.I., Tchoubar, C., Drits, V.A. (1983): Use of diffraction and Mössbauer methods for the structural and crystal-chemical characterization of nontronite. *J. Appl. Crystallogr.*, **16**, 374–383.

Bookin, A.S., Dainyak, L.G., Drits, V.A. (1978): Interpretation of the Mössbauer spectra of layer silicates on the basis of structural modelling. *Phys.Chem. Minerals*, **3**, 58–59.

Brese, N.E. & O'Keefe, M. (1991): Bond-valence parameters for solids. *Acta Crystallogr.*, **B47**, 192–197.

Brown, I.D. (1981): The bond-valence method: an empirical approach to chemical structure and bonding. *In* "Structures and bonding in crystals", M. O'Keefe, A. Navrotsky (eds), Academic Press, New York, 1–30.

– (1992): Chemical and steric constraints in inorganic solids. *Acta Crystallogr.,* **B48**, 553–572.

Brown, I.D. & Altermatt, D. (1985): Bond-valence parameters obtained from a systematic analysis of the inorganic crystal structure database. *Acta Crystallogr.*, **B41**, 244–247.

Brown, I.D. & Shannon, R.D. (1973): Empirical bond-strength-bond-length curves for oxides. *Acta Crystallogr.*, **A29**: 266–282.

Coey, J.M.D. (1980): Clay Minerals and their transformations studied with nuclear techniques: The contribution of Mössbauer spectroscopy. *Atomic Energy Rev.*, **18**, 73–124.

Coey, J.M.D., Chukhrov, F.D., Zvyagin, B.B. (1984): Cation distribution, Mössbauer spectra, and magnetic properties of ferripyrophyllite. *Clays Clay Minerals*, **32**, 198–204.

Cuadros, J. (2002): Structural insights from the study of Cs-smectites submitted to wetting-and-drying cycles. *Clay Minerals*, **37**, 471–486.

Dainyak, L.G. (1980): Interpretation of Mössbauer spectra of Fe^{3+}-bearing layer silicates on the base of structural modelling. PHD Thesis, Geological Institute, Academy of Sciences of USSR, Moscow (in Russian).

Dainyak, L.G. & Drits, V.A. (1987): Interpretation of the Mössbauer spectra of nontronite, celadonite, and glauconite. *Clays Clay Minerals*, **35**, 363–372.

Dainyak, L.G., Bookin, A.S., Drits, V.A., Tsipursky, S.I. (1981): Mössbauer and electron diffraction study of cation distribution in celadonite. *Acta Crystallogr.*, **A-37** (suppl.), C-362.

Dainyak, L.G., Bookin, A.S., Drits, V.A. (1984a): Interpretation of Mössbauer spectra of dioctahedral Fe^{3+}-containing 2:1 layer silicates. II. Nontronite. *Kristallografiya*, **29**, 304–311 (in Russian).

–, –, – (1984b): Interpretation of Mössbauer spectra of dioctahedral Fe^{3+}-containing 2:1 layer silicates. III. Celadonite. *Kristallografiya*, **29**, 312–321 (in Russian).

Dainyak, L.G., Bookin, V.A., Drits, V.A., Dainyak, B.A. (1984c): Interpretation of Mössbauer spectra of dioctahedral Fe^{3+}-containing 2:1 layer silicates. I. Computation of electric field gradients on the basis of structural modelling. *Kristallografiya*, **29**, 94–100 (in Russian).

Dainyak, L.G., Drits, V.A., Heifits, L.M. (1992): Computer simulation of cation distribution in dioctahedral 2:1 layer silicates using IR data: Application to Mössbauer spectroscopy of a glauconite sample. *Clays Clay Minerals*, **40**, 470–479.

Drits, V.A. (1975): Structural and crystal chemical peculiarities of layer silicates. *In* Crystal Chemistry of Minerals and Problems of Geology, Nauka, Moscow, 35–51 (in Russian).

Drits, V.A. & Kossovskaya, A.G. (1992): Layer silicates: micas, chlorites. Nauka, Moscow, 180 p. (in Russian).

Drits, V.A. & McCarty, D.K. (1996): The nature of diffraction effects from illite and illite-smectite consisting of interstratified trans-vacant and cis-vacant layers: A semiquantitative technique for determination of layer-type content. *Amer. Mineral.*, **81**, 852–863.

Drits, V.A., Kameneva, M.Yu., Sakharov, B.A., Dainyak, L.G., Tsipursky, S.I., Smoliar, B.B., Bookin, A.S., Salyn, A.L. (1993): Actual Structure of Glauconites and Related Dioctahedral 2:1 Varieties. Nauka, Novosibirsk (in Russian).

Drits, V.A., Tsipursky, S.I., Plancon, A. (1984): Application of the method for the calculation of intensity distribution to electron diffraction structural analysis. *Izvestia Acad. Nauk SSSR, seria physicheskaia*, **2**, 1707–1713 (in Russian).

Drits, V.A., Dainyak, L.G., Muller, F., Besson, G., Manseau, A. (1997): Isomorphous cation distribution in celadonites, glauconites, and Fe-illites determined by infrared, Mössbauer and EXAFS spectroscopies. *Clay Minerals*, **32**, 153–179.

Drits, V.A., Sakharov, B.A., Dainyak, L.G., Salyn, A.L., Lindgreen, H. (2002): Structural and chemical heterogeneity of illite-smectites from Upper Jurassic mudstones of East Greenland related to

volcanic and weathered parent rocks. *American Mineral.*, **87**, 1590–1607.

Goodman, B.A. (1976a): The effect of lattice substitutions on derivation of quantitative site populations from the Mössbauer spectra of 2:1 layer lattice silicates. *J. Phys.*, **37**: C6–819–823.

– (1976b): The Mössbauer spectrum of a ferrian muscovite and its implications in the assignment of sites in dioctahedral micas. *Minaral. Mag.*, **40**, 513–517.

– (1987): On the use of Mössbauer spectroscopy for determinig the distribution of iron in aluminosilicate minerals. *Clay Minerals*, **22**, 363–366.

Greenwood, N.N. & Gibb, T.C. (1971): Mössbauer Spectroscopy. Chapman and Hall, London, 659 p.

Heller-Kallai, L. & Rozenson, I. (1981): The use of Mössbauer spectroscopy of iron in clay mineralogy. *Phys. Chem. Minerals*, **7**, 223–238.

Huggins, F.E. (1976): Mössbauer studies of iron minerals under pressures of up to 200 kbars. *In* "The physics and chemistry of minerals and rocks", R.G.J. Strens (ed), John Wiley, New York, 613–640.

Ingalls, R. (1964): Electric-field gradients tensor in ferrous compounds. *Phys. Rev.*, **133**, A787-A795.

Ivanovskaya, T.A., Tsipirsky, S.I., Yakovleva, O.V. (1989): Mineralogy of globular glauconites from Vendian and Rephean of the Urals and Siberia. *Litologiya i poleznie iskopaemie*, **3**, 83–89 (in Russian).

Johnston, J.H. & Cardile, C.M. (1985): Iron sites in notronite and effect of interlayer cations from Mössbauer spectra. *Clays Clay Minerals*, **33**, 21–30.

Kroll, H., Maurer, H., Stöckelmann, D., Beckers, W., Fulst, J., Krüsemann, R., Stutenbäumer, T., Zingel, A. (1992): Simulation of crystal structures by a combined distance-least-squares/valence-rule method. *Z. Kristallogr.*, **199**, 49–66.

Lindgreen, H., Jacobsen, H., Jacobsen, H.J. (1991): Diagenetic structural transformations in North Sea Jurassic illite/smectite. *Clays Clay Minerals*, **39**, 54–69.

Manceau, A., Chateigner, D., Gates, W.P. (1998): Polarized EXAFS, distance-valence least-squares modeling (DVLS), and quantitative texture analysis approaches to the structural refinement of Garfield nontronite. *Phys. Chem. Minerals*, **25**, 347–365.

Manceau, A., Lanson, B., Drits, V.A., Chateigner, D., Gates, W.P., Wu, J., Huo, D., Stucki, J.W. (2001): Oxidation-reduction mechanism of iron in dioctahedral smectites: 1. Crystal chemistry of oxidized reference nontronites. *Amer. Mineral.*, **85**, 133–152.

Mineeva, R.M. (1978): Relationship between Mössbauer spectra and defect structure in biotites from electric field gradient calculation. *Phys. Chem. Minerals*, **2**, 267–277.

Muller, F., Drits, V.A., Plancon, A., Besson G. (2000): Dehydroxylation of Fe^{3+}, Mg-rich dioctahedral micas: (I) structural transformation. *Clay Minerals*, **35**, 491–504.

Nikolaeva, I.V. (1977): Glauconite group minerals of sedimentory formations. Proc. Institute of Geology and Geophysics RAS, Nauka, Novosibirsk, 328 p. (in Russian).

Parker, S.C., Calton, C.R.A., Cormark, A.N. (1984): Structure prediction of silicate minerals using energy-minimization techniques. *Acta Crystallogr.*, **40**, 200–208.

Pavlishin, V.I., Platonov, A.N., Polshin, E.V., Semenova, T.F., Starova, G.K. (1978): Micas with iron in tetrahedral coordination. *Zapiski Vsesoyuznogo Mineralogicheskogo obshestva*, **107**, 165–175 (in Russian).

Popov, V.I., Khramov, D.A., Lobanov, F.I. (1988): Absorber shape: The influence on the Mössbauer spectrum parameters. *In* Proc. of USSR Conference on Applied Mössbauer Spectroscopy "Volga", Moscow Physical Engineering Inst., Moscow, 32–33 (in Russian).

Rancourt, D.G. & Ping, J.Y. (1991): Voigt-based methods for arbitrary-shape static hyperfine parameter distribution in Mössbauer spectroscopy. *Nucl. Instrum. Method Phys. Res.*, **b58**, 85–97.

Raskazov, A. (1984): Clay minerals of potassium-bearing deposits. Nauka, Moscow, 73 p. (in Russian).

Redhammer, G.J. (1998): Characterisation of synthetic trioctahedral micas by Mössbauer spectroscopy. *Hyperfine Interactions*, **117**, 85–115.

Redhammer, G.J., Beran, A., Schneider, J., Amthauer, G., Lottermoser, W. (2000): Spectroscopic and structural properties of synthetic micas on the annite-siderophyllite binary: Synthesis, crystal structure refinement, Mössbauer, and infrared spectroscopy. *Amer. Mineral.*, **85**, 449–465.

Redhammer, G.J., Amthauer, G., Lottermoser, W., Roth, G. (2002): Quadrupole Splitting Distribution of Fe^{2+} in Synthetic Trioctahedral Micas. *Hyperfine Interactions*, **141/142**, 345–349.

Rusakov, V.S. (2000): Methods to deriving information from Mössbauer spectra of locally inhomogeneous systems (Complex MS Tools). *In* "Mössbauer spectroscopy of locally inhomogeneous systems", Alma-Ata, 11–86 (in Russian).

Rusakov, V.S. & Chistyakova, N.I. (1992): Mössbauer Program Complex MS Tools. Latin American Conference on Applications of the Mössbauer Effect, LACAME'92. Buenos Aires. Argentina, N° 7, 3.

Sainz-Diaz, C.I., Timon, V., Bodella, V., Hernandez-Laguna, A. (2000): Study of the OH group properties in octahedral sheet of phyllosilicates by using computational chemistry methods. *Amer. Chem. Soc. Natl. Meet., Ext. Abstract, Am. Chem. Soc., Div. Envision*, **40** (1), 340–341.

Sainz-Diaz, C.I., Cuadros, J., Hernandez-Laguna, A. (2001): Analysis of cation distribution in the octahedral sheet of dioctahedral 2:1 phyllosilicates by using inverse Monte Carlo methods. *Phys. Chem. Minerals*, **28**, 445–454.

Sakharov, B.A., Besson, G., Drits, V.A., Kameneva, M.Y., Salyn, A.L., Smolyar, B.B. (1990): X-ray study of the nature of stacking faults in the structure of glauconites. *Clay Minerals*, **25**, 419–435.

Shabani, A.A.T., Rancourt, D.G., Lalonde, A.E. (1998): Determination of cis and trans Fe^{2+} populations in $2M_1$ muscovite by Mössbauer spectroscopy. *Hyperfine Interactions*, **117**, 117–129.

Shutov, V.D., Drits, V.A., Kats, M.Ya., Sokolova, A.L. (1975): Crystal chemistry of glauconites as indicator of facial conditions of formation and postsedimentary transformation of these minerals. *In* "Crystal Chemistry of Minerals and Geological Problems", A.G. Kossovskaya (ed), Nauka, Moskva (in Russian).

Slonimskaya, M.V., Besson, G., Dainyak, L.G., Tchoubar, C., Drits, V.A. (1986): The interpretation of the IR spectra of celadonites and glauconites in the region of the OH stretching frequences. *Clay Minerals*, **21**, 377–388.

Smoliar-Zviagina, B.B. (1993): Relationships between structural parameters and chemical composition of micas. *Clay Minerals*, **28**, 603–624.

Townsend, M.G., Longworth, G., Ross, C.A.M., Provencher, R. (1987): Ferromagnetic or antiferromagnetic Fe III spin configurations in sheet silicates. *Phys. Chem. Minerals*, **15**, 64–70.

Tsipursky, S.I. & Drits, V.A. (1984): The distribution of octahedral cations in the 2:1 layers of dioctahedral smectites studied by oblique-texture electron diffraction. *Clay Minerals*, **19**, 177–193.

Tsipursky, S.I., Drits, V.A., Plancon, A. (1985): Calculation of the intensities distribution in oblique texture electron diffraction patterns. *Kristallografiya*, **30**, 38–44 (in Russian).

Received 28 April 2003
Modified version received 25 November 2003
Accepted 26 January 2004